 FDMP, vol.6, no.1, pp.41-73, 2010

Thermocapillary and Natural Convection in Double Layer Systems of Herschel-Bulkley and Newtonian Fluids, Exact Solutions

O.M. Lavrenteva, Yu. Holenberg and A. Nir[1]

Abstract: A variety of exact analytical solutions describing natural and thermocapillary convection in a horizontal double layer system consisting of Newtonian and Herschel-Bulkley fluids subjected to longitudinal temperature and concentration gradients is constructed. The lower boundary of the system is a solid wall with no-slip, while the upper ones if either a solid wall or a free surface. It was demonstrated that, depending on the governing parameters of the system, viscoplastic layer is entirely yielded or unyielded, or it can be yielded partially, exhibiting up to 5 flowing and quasi-solid layers. The dependence of the flow patterns (appearance and position of unyielded regions), velocity and temperature profiles, on the governing parameters have been studied.

Keywords: Viscoplastic fluid, liquid layer, convection, Marangoni flow

1 Introduction

Viscoplastic media exhibit a solid-like behavior being exposed to low levels of stress and flow if the stress level exceeds a critical value, commonly known as the yield stress. Such materials appear in various natural phenomena as well as in a variety of technological applications. Known yield-stress fluids include mud, cements, lava, glues and paints, various food stuffs, fermentation broths, foams, suspensions, emulsions, gels, rocket fuels and other polymer mixtures. Many biological tissues exhibit viscoplastic behavior as well.

The analysis of the mechanics of yield stress materials has been of continuous interest since the pioneering work of Bingham (1922), and several invariant models for the rheology were formulated throughout the years (see e.g. Oldroyd (1947a,b) and Prager (1954)). A popular generalization of the Bingham constitutive description is known as the Herschel-Bulkley model (see, e.g. Burgos, Alexandrou and Entov, 1999).

[1] Chemical Engineering Dept, Technion, Israel

Many natural and industrial processes involve combined motion of yield stress and Newtonian media, such as flow of the water over mud bottom, co-extrusion in bi and multi layer polymer film production or gravity-induced sedimentation or rise of drops and bubbles in a viscoplastic material. Frigaard (2001) and Moyers-Gonzalez, Frigaard, and Nouar (2004) have demonstrated that using of viscoplastic lubricant can stabilize multi layer sheared flows. These theoretical findings were recently approved experimentally by Huen, Frigaard and Martinez (2007).

A number of results are available that concern the behavior of bubbles in a yield stress medium. One of the early studies of fluid particle dynamics in yield stress materials was reported by Bhavaraju, Mashelkar and Blanch (1978), who employed perturbation in the Bingham parameter to study the motion of a non-deformable bubble in an unbounded medium. Stein and Buggish (2000) applied perturbation techniques to demonstrate that bubbles trapped in visco-plastic medium can be made to rise by applying an external oscillatory pressure and reported experimental results confirming these predictions. Vasil'chenko and Potapov (1996) studied the rise of large bubbles in a column filled with a viscoplastic fluid (with bubble length scale being comparable or larger than the column radius) and observed that the bubble rise velocity became constant beyond a certain size. A recent work by Dubash and Frigaard (2004) addresses the buoyancy-induced motion of deformable bubbles and uses variational principles (Prager, 1954) to establish bubbles stopping conditions. Experiments involving the rise of air bubbles in a column of viscoplastic fluid (Carbopol solution) are reported by Dubash and Frigaard (2007).

The motion of viscous inclusions in yield stress environment attracted less attention so far. Numerical simulations of deformation and rupture of a viscous drop in an entirely yielded Bingham liquid was reported by Li and Renardy (2000). Simulations of axisymmetric gravity-induced settling of single and multiple interacting deformable viscous drops in a Bingham fluid were performed by Potapov, Spivak, Lavrenteva and Nir (2006). The focus of this study was on the influence of the drops deformations on the shape and extent of the yield regions and on the velocities of the drops. Recently Singh and Denn (2008) reported a numerical study of the buoyancy-driven motion of bubbles and droplets in a Bingham fluid in two-dimensional geometry that enables to explore non-axisymmetric configurations.

Numerous industrial processes and physical applications involving yield stress materials are accompanied by intensive heat and mass transfer and, thus, the study of convective motion of such media is important. Cherkasov (1979) and Lyubimova and Lyubimov (1980) investigated free and induced convection of Bingham plastic in vertical layers. Nouar (2008) studied the combined forced and free convection heat transfer of a yield stress fluid in a horizontal duct heated uniformly with a constant heat flux density. A recent paper by Metivier and Nouar (2008) is devoted to

the onset of the Rayleigh-Benard thermal convection cells for a horizontal layer of viscoplastic fluid heated from below and for which an axial laminar flow is added.

Most of the studies of the motion of viscoplastic fluids are focused on macro scale flows, where capillary effects on the viscoplastic-fluid interfaces are minor and, thus, these effects in application to yield stress media are almost unstudied so far. However, at smaller scales, capillary and thermocapillary effects are expected to be important, especially for processes accompanied by intensive heat or mass transfer.

We report on a variety of exact analytical solutions describing natural and thermocapillary convection in a horizontal double layer system consisting of Newtonian and Herschel-Bulkley fluids subjected to a longitudinal temperature and concentration gradients. The dependence of the flow patterns (appearance and position of unyielded regions), velocity, temperature and concentration profiles on the governing parameters have been studied. The constructed solutions generalize the well–known Birikh (1966) solution, where the velocity is directed horizontally and depends on a vertical coordinate, y, while the temperature and concentration fields are sums of linear functions of a horizontal coordinate, x, and non-linear functions of y. Birikh solutions were generalized to a two-layer flow by Napolitano (1980) and to 3D case by Pukhnachov (2000). Note that most studies of this type of flow assume non-deformable interfaces, neglecting normal stress balance. Recently, Goncharova and Kabov (2009) constructed Birikh type solutions satisfying all exact conditions at the interfaces between liquid and co-current gas flow and demonstrated that the gas flow can be used to control convection in liquid. In this work we follow the approach of Goncharova and Kabov (2009).

Physical and mathematical formulations for the problem under consideration are presented in section 2. Basic equations, boundary conditions, scaling, governing parameters and special type of solutions are introduced. In section 3, various possible regimes of the flow in viscoplastic layer are described and their dependence on governing parameters is studied. In sections 4 and 5, results of computations of velocity, temperature and concentration profiles for various sets of governing parameters are presented and discussed for the cases of free and solid upper boundary of the system. Conclusions and discussion of possible further generalizations of the results are given in section 6.

2 Problem formulation

Consider a horizontal two-layer system of an infinite extent in the longitudinal direction x lying on a rigid plane $y = -d_{HB}$, see Fig. 1.

From above the system is bounded at $y = d_N$ either by a solid wall, or by a free boundary. The upper and lower layer consist of Newtonian and Herschel-Bulkley

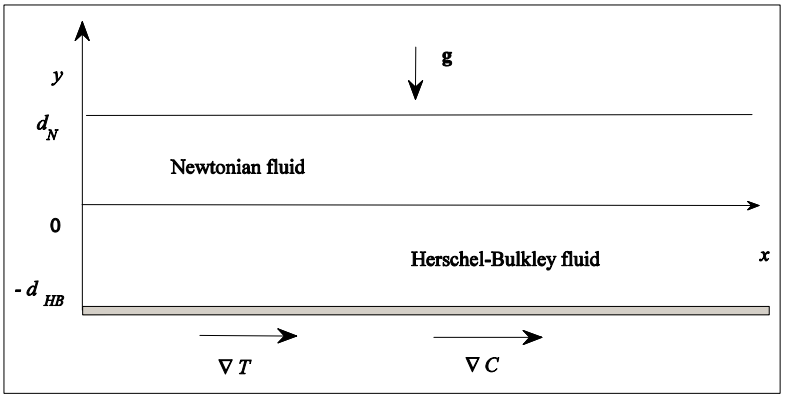

Figure 1: System schematics.

fluid, respectively. The temperature, T, and the concentration of a soluble substance, C, in the vicinity of the bottom are linear in x,

$$T = T_0 + a_T x, \quad C = C_0 + a_C x, \quad y = -d_{HB}. \tag{1}$$

The surface tensions at the interface, σ_{HB}, and at the free boundary, σ_N, are assumed to be linear with temperature and concentration

$$\sigma_m = \sigma_{m,0} + \sigma_{m,C}(C - C_0) + \sigma_{m,T}(T - T_0), \quad m = N, HB. \tag{2}$$

The flow is due to density gradient and thermo-capillary (Marangoni) effect at the free boundary and the interface of the two fluids.

Adopting the Boussinesq approximation, the governing momentum and continuity equations are of the form:

$$\begin{aligned} &\rho_{0,m}\left(\frac{\partial U_i}{\partial t} + U_k\frac{\partial U_i}{\partial x_k}\right) = -\frac{\partial p}{\partial x_i} + \rho_{0,m} g_i\left(\beta_m^C(C - C_0) + \beta_m^T(T - T_0)\right) + \frac{\partial \tau_{ik}}{\partial x_k}, \\ &\frac{\partial U_i}{\partial x_i} = 0, \quad \mathbf{x} \in \Omega_m, \quad m = N, HB. \end{aligned} \tag{3}$$

Here $\boldsymbol{U}$ denotes fluid velocity, $\boldsymbol{g}$ is the gravitation acceleration, $\rho_{0,m} = \rho_m(T_0, C_0)$ is fluid density at temperature T_0 and concentration C_0,

$$\beta_m^C = \frac{1}{\rho_{0,m}}\left.\frac{\partial \rho_m}{\partial C}\right|_{C=C_0, T=T_0}, \quad \beta_m^T = \frac{1}{\rho_{0,m}}\left.\frac{\partial \rho_m}{\partial T}\right|_{C=C_0, T=T_0},$$

$m = N$ for the Newtonian fluid and m=HB for the Herschel-Bulkley fluid, p is the dynamic pressure and $\boldsymbol{\tau}$ is the excess stress tensor. For the Newtonian fluid $\boldsymbol{\tau} = \mu_N \mathbf{D}$, while for the Herschel-Bulkley viscoplastic medium

$$\begin{cases} \boldsymbol{\tau} = \left(K\,|\mathbf{D}|^{(n-1)} + \frac{\tau_Y}{|\mathbf{D}|} \right) \mathbf{D} & |\boldsymbol{\tau}| > \tau_Y, \\ \mathbf{D} = \mathbf{0} & |\boldsymbol{\tau}| < \tau_Y, \end{cases} \tag{4}$$

Here $\mathbf{D}$ is the rate of strain tensor, $D_{ij} = (\partial U_i/\partial x_j + \partial U_j/\partial x_i)$ and $|\mathbf{A}| = \sqrt{\sum A_{ij}^2/2}$ denotes a second invariant of a tensor $\mathbf{A}$. THe rheological parameters of a Herschel-Bulkley fluid are the yield stress,τ_Y, the consistency factor,K, and the power law index, n. The viscosity of Newtonian fluid is denoted by μ_N.

Mass and heat transfer is governed by

$$\begin{aligned} &\frac{\partial C}{\partial t} + U_i \frac{\partial C}{\partial x_i} = \frac{\partial}{\partial x_i} \left(D_m \frac{\partial C}{\partial x_i} + D_m^T \frac{\partial T}{\partial x_i} \right), \\ &\rho_{0,m} c_p \left(\frac{\partial T}{\partial t} + U_i \frac{\partial T}{\partial x_i} \right) = \frac{\partial}{\partial x_i} \left(\kappa_m \frac{\partial T}{\partial x_i} \right), \quad \mathbf{x} \in \Omega_m, \quad m = N, HB. \end{aligned} \tag{5}$$

Here D, D^T and κ denote diffusivity, thermo-diffusivity coefficient and thermal conductivity, respectively. At the bottom no slip boundary conditions

$$\mathbf{U} = \mathbf{0}, \tag{6}$$

are satisfied, while the temperature and concentration are of the form (1).

At the inter interface separating the two layers Γ_{HB}, the velocity is continuous

$$[\mathbf{U}] = \mathbf{0}, \quad \mathbf{x} \in \Gamma_{HB}, \tag{7}$$

and the dynamic conditions are satisfied,

$$\begin{aligned} &[\tau_{ik}]\,\hat{t}_i \hat{n}_k - \sigma_{HB,T} \frac{\partial T}{\partial x_i} \hat{t}_i - \sigma_{HB,C} \frac{\partial C}{\partial x_i} \hat{t}_i = 0, \\ &-[p] + [\tau_{ik}]\,\hat{n}_i \hat{n}_k = H_{HB} \sigma_{HB}, \quad \mathbf{x} \in \Gamma_{HB}. \end{aligned} \tag{8}$$

Here and below [ ] denotes jump at the interface, while $\hat{\mathbf{n}}$ and $\hat{\mathbf{t}}$ are normal and tangential unit vectors, respectively, H is the mean curvature of the surface.

Temperature, heat and mass fluxes are continuous at the interface, while the concentrations in the two layers are in local thermodynamic equilibrium,

$$\begin{aligned} &[T] = 0, \quad C_N = \alpha_{eq} C_{HB}, \quad \left[\kappa \frac{\partial T}{\partial x_i} \right] \hat{n}_i = 0, \\ &\left[D \frac{\partial C}{\partial x_i} + D^T \frac{\partial T}{\partial x_i} \right] \hat{n}_i = 0, \quad \mathbf{x} \in \Gamma_{HB}, \end{aligned} \tag{9}$$

where α_{eq} is the equilibrium constant.

The upper boundary of the double layer is either a free surface or a solid wall. In the first case, the boundary conditions are

$$\begin{aligned} &\tau_{ik}\hat{l}_i\hat{n}_k + \sigma_{N,T}\frac{\partial T}{\partial x_i}\hat{t}_i + \sigma_{N,C}\frac{\partial C}{\partial x_i}\hat{t}_i = 0, \\ &-p + \tau_{ik}\hat{n}_i\hat{n}_k = H_N\sigma_N - p_0, \end{aligned} \tag{10}$$

$$\kappa_N\frac{\partial T}{\partial x_i}\hat{n}_i = Q_T, \quad \left(D_N\frac{\partial C}{\partial x_i} + D_N^T\frac{\partial T}{\partial x_i}\right)\hat{n}_i = Q_C, \quad \mathbf{x}\in\Gamma_N. \tag{11}$$

In the case of a solid upper boundary, conditions (10) are replaced by the no-slip conditions

$$\mathbf{U} = \mathbf{0}, \quad \mathbf{x}\in\Gamma_N. \tag{12}$$

For the temperature and concentration, we either consider the condition (11), or replace one or both of these by the first order conditions

$$T = T_1 + a_T x, \quad C = C_1 + a_C x, \quad \mathbf{x}\in\Gamma_N. \tag{13}$$

We are looking for stationary solutions of the problems (1)-(11) and (1)-(9), (12), (13) in the form

$$\begin{aligned} &\mathbf{U} = (V(y),0,0), \quad T = T_0 + a_T x + \Theta(y), \quad C = C_0 + a_C x + \Phi(y), \\ &\tau_{xx} = \tau_{yy} = \tau_{xz} = \tau_{yz} = \tau_{zz} = 0, \quad \tau_{xy} = \tau(y), \quad p = f(y)x + P(y), \end{aligned} \tag{14}$$

with boundaries Γ_{HB} and Γ_N being the planes y= 0 and $y = d_N$, respectively.

Introduce dimensionless variables scaling the length with Herschel-Bulkley fluid layer depth d_{HB}, stress, pressure and $P_m(y)$ function with the characteristic stress induced by the density variations in viscoplastic medium,

$$\tau^* = \left|\left(a_T\beta_{HB}^T + a_C\beta_{HB}^C\right)g\rho_{0,HB}d_{HB}^2\right|.$$

The function $f(y)$ is scaled with τ^*/d_{HB}, velocity with $V^* = d_{HB}(\tau^*/K)^{1/n}$ and temperature with $T^* = |a_T d_{HB}|$. The concentration is scaled by its characteristic change at the length scale, C^*, which equals $|a_C d_{HB}|$ if $a_C \neq 0$ and $|C_1 - C_0|$ or $|Q_C d_{HB}|$ in the opposite case. For simplicity of presentation, the notations for scaled variables are the same as for the original dimensional ones. Thus, the lower viscoplastic and upper Newtonian fluids occupy the domains $(1,0)$ and $(0,d)$, respectively, with $d = d_N/d_{HB}$.

It follows from the momentum equations that

$$f(y) = \delta_m y - B_m, \tag{15}$$

and, hence,

$$\tau(y) = \frac{\delta_m y^2}{2} - B_m y + M_m, \quad y \in \Omega_m, \quad m = N, HB, \tag{16}$$

where

$$\delta_{HB} = 1, \quad \delta_N = \delta = \frac{a_T \beta_N^T + a_C \beta_N^C}{a_T \beta_{HB}^T + a_C \beta_{HB}^C}, \tag{17}$$

while B_m and $M_m\,(m = N, HB)$ are constants of integration to be determined from the boundary conditions. The choice $\delta_{HB} = 1$ corresponds to the choice of the x axis direction such that the density of the Herschel-Bulkley fluid increases with x. Scaled stress and velocity field are related by

$$\begin{cases} \tau = \left|\frac{dV}{dy}\right|^{n-1} \frac{dV}{dy} + Bn\,\mathrm{sign}\left(\frac{dV}{dy}\right), & |\tau| > Bn, \\ \frac{dV}{dy} = 0, & |\tau| \le Bn, \end{cases} \tag{18}$$

for the viscoplastic medium, and by

$$\tau = \mu \frac{dV}{dy}, \tag{19}$$

for the Newtonian fluid. Here

$$Bn = \frac{\tau_Y}{\tau^*}, \quad \mu = \frac{\mu_N V^*}{d_{HB} \tau^*}. \tag{20}$$

Solving (18) and (19) with respect to dV/dy leads to

$$\begin{aligned} &\frac{dV}{dy} = \mathrm{sign}(\tau(y))\,[\max(|\tau(y)| - Bn, 0)]^{1/n}, \quad y \in (-1, 0), \\ &\frac{dV}{dy} = \frac{1}{\mu}\tau(y), \quad y \in (0, d). \end{aligned} \tag{21}$$

Substituting the presentation (14) into the transport equations (5) results in the following equations for the functions $\Theta(y)$and$\Phi(y)$

$$\frac{d^2\Theta}{dy^2} = Pe_m^T V, \quad \frac{d^2\Phi}{dy^2} = Pe_m^C V, \tag{22}$$

where

$$Pe_m^T = \frac{\rho_{0,m} c_{pm} V^* d_{HB}}{\kappa_m}, \quad Pe_m^C = \frac{V^* a_C d_{HB}^2}{C^* D_m} - \frac{a_C d_{HB} D_m^T}{C^* D_m} Pe_m^T. \tag{23}$$

Note that while Pe_m^T is always positive,Pe_m^C can be negative as well.
Function $P(y)$ that determines the pressure distribution satisfies

$$\frac{dP(y)}{dy} = g\rho_{0,m}\left[\beta_m^C \Phi(y) + \beta_m^T \Theta(y)\right], \tag{24}$$

Boundary conditions at the bottom, y = – 1, are

$$V_{HB}(-1) = 0; \quad \Theta_{HB}(-1) = 0; \quad \Phi_{HB}(-1) = 0. \tag{25}$$

At the interface, y = 0,

$$\begin{aligned}
&\tau_{HB}(0) - \tau_N(0) = Ma_{HB} = \left(\sigma_{HB}^C a_T + \sigma_{HB}^C a_C\right)/\tau^*, \quad V_{HB}(0) = V_N(0), \\
&\Theta_{HB}(0) = \Theta_N(0), \quad \Phi_{HB}(0) = \alpha_{eq}\Phi_N(0), \quad \Theta'_{HB}(0) = \kappa\Theta'_N(0), \quad P_N(0) = P_{HB}(0), \\
&\Phi'_{HB}(0) + \frac{D_{HB}^T T^*}{D_{HB} C^*}\Theta'_{HB}(0) = \frac{D_N}{D_{HB}}\Phi'_N(0) + \frac{D_N^T T^*}{D_{HB} C^*}\Theta'_N(0), \quad f_N(0) = f_{HB}(0).
\end{aligned} \tag{26}$$

At the upper free boundary $y = d$,

$$\begin{aligned}
&\tau_N(d) = Ma_N = \left(\sigma_N^C a_T + \sigma_N^C a_C\right)/\tau^*; \quad P(d) = P_0 = p_{atm}/\tau^*, \quad f(d) = 0, \\
&\Theta'_N(d) = q_T = \frac{Q_T}{\kappa_N a_T}, \quad \Phi'_N(d) + \frac{D_N^T T^*}{D_N C^*}\Theta'_N(d) = q_C = \frac{Q_C d_{HB}}{D_N C^*}.
\end{aligned} \tag{27}$$

In the case of an upper solid wall, at $y = d$, the velocity vanishes,

$$V_N(d) = 0. \tag{28}$$

For the heat and mass transport at the upper solid wall, we specify either heat and mass fluxes, resulting in boundary conditions analogous to (27), or temperature and concentration distribution analogous to that at the bottom.

$$\Theta_N(d) = \theta = T_1/T^*, \quad \Phi_N(d) = \phi = C_1/C^*. \tag{29}$$

The velocity field is governed by 7 parameters, Ma_{HB}, Ma_N, δd, Bn, μ, and n for the case of free boundary, and by the same parameters except for Ma_N for flow between two parallel solid walls.

The first and the last of the conditions (26) yield that $M_{HB} = M = M_N + Ma_{HB}$ and $B_N = B_{HB} = B$, respectively. The stress distribution is, thus,

$$\tau_{HB}(y) = \frac{y^2}{2} - By + M, \quad \tau_N(y) = \frac{\delta y^2}{2} - By + M - Ma_{HB}. \tag{30}$$

The problem is reduced to finding two constants, B and M, and the functions $V_m(y)$, $\Phi_m(y)$, $\Theta_m(y)$ and $P_m(y)$, satisfying equations (21), (22) and (24) with $\tau_m(y)$ given by (30) and boundary conditions (25)–(27) or (25), (26), (28) and (29).

3 Regimes of the flow in the viscoplastic layer.

The viscoplastic fluid is yielded if $|\tau_{HB}| > Bn, y \in (-1,0)$, with τ_{HB} given by (30). Hence, the regime of the flow is determined by a relation between 3 parameters: B, M and Bn. The Herschel-Bulkley medium flows or remains quiescent near the bottom if $|\tau_{HB}(-1)| = |M + B + 1/2| > Bn$, or $|M + B + 1/2| \leq Bn$,respectively. Similarly, the viscoplastic fluid is yielded or unyielded near the interface if $|\tau_{HB}(0)| = |M| > Bn$, or $|M| \leq Bn$, respectively. Since τ_{HB} is a square polynomial in y, it has a single minimum at $y = B$. If this minimum is located inside the domain occupied by the Herschel-Bulkley medium, $-1 < B < 0$, and $|\tau_{HB}(B)| = \left|B^2/2 - M\right| > Bn$, a domain of yielded fluid is present inside the viscoplastic layer, which may be unyielded near the bottom and the interface. Similarly, if $-1 < B < 0$, and $\left|B^2/2 - M\right| < Bn$, a domain of unyielded fluid is present inside the Herschel-Bulkley layer, which may be yielded near the bottom and the interface. It is easy to see that 9 different regimes of the flow with up to 5 alternating yielded and unyielded layers are possible:

1. Entirely yielded, 1a: $M < \min(-Bn, -B - 1/2 - Bn)$ or $M > Bn$, $B > 0$ or $M > -B - 1/2 + Bn$, $B < -1$, or $B^2/2 > M + Bn$, $B \in [-1,0]$.

2. Entirely unyielded, 1b: $M < \min(Bn, -B - 1/2 + Bn)$ or $-B - 1/2 - Bn < M < Bn$ or $-Bn < M < -B - 1/2 + Bn$ or $B^2/2 - Bn < M < \min(-B - 1/2 + Bn, Bn)$. This regime is possible solely if $Bn > 1/16$, i.e. if the stresses induced by density variation are not strong enough to yield the fluid.

3. Two layers, lower one is yielded, 2a: $|\tau_{HB}(0)| = |M| \leq Bn$ and $M < -B - 1/2 - Bn$, or $\max(B^2/2 - Bn, -B - 1/2 + Bn) < M < Bn$, $B < 0$, or $\max(-Bn, -B - 1/2 + Bn) < M < Bn$, $B > 0$.

4. Two layers, lower one is unyielded, 2b: $|\tau_{HB}(-1)| = |M + B + 1/2| \leq Bn$ and $\{M < -Bn$ or $(M > \max(B^2/2 - Bn, Bn)$, $B > -1)$ or $B < -1\}$.

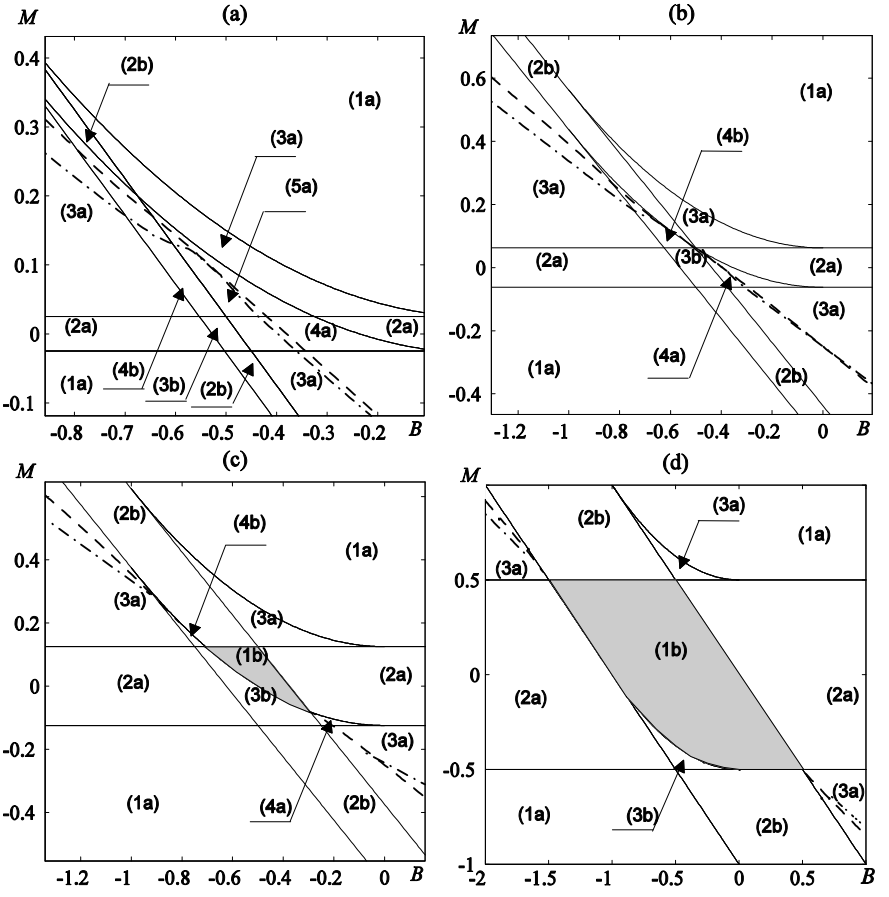

Figure 2: Maps of flow regimes in (B,M) parametric plane at various Bingham numbers. (a) Bn = 1/36, (b) Bn = 1/16; (c) Bn = 1/8; (d) Bn = 1/2. Na and Nb correspond to a N-layer regime with yielded and unyielded lowest layer, respectively. Boundaries between domains of different regimes are marked by solid lines. Dashed and dashed-dotted lines are the curves $Q_{HB}(B,M,n,Bn) = 0$ for n= 1 and n= 1/4, respectively.

5. Three layers, lower one is yielded, 3a: $Bn - B - 1/2 < M < -Bn$ or $(-1 < B < 0$ and $\max(B^2/2 - Bn, Bn, Bn - B - 1/2) < M < B^2/2 + Bn.)$ or $Bn < M < -Bn - B - 1/2$.

6. Three layers, lower one is unyielded, 3b: $-B < M < \min(B^2/2 - Bn, Bn, Bn - B - 1/2)$ and $-1 < B < 0$.

7. Four layers, lower one is yielded, 4a: $-1 < B < 0$ and $\max(Bn-B-1/2, -Bn) < M < \min(B^2/2-Bn, Bn)$.

8. Four layers, lower one is unyielded, 4b: $Bn < M < \min(B^2/2-Bn, Bn-B-1/2)$, $-1 < B < 0$.

9. Five layers, lower one is yielded, 5a: $\max(Bn, -B-1/2+Bn) < M < B^2/2-Bn$, $-1+2\sqrt{Bn} < B < -2\sqrt{Bn}$.

Maps of possible flow regimes at (B,M) plane for various constant Bn are presented in Fig. 2. Fig. 2a corresponds to the cases of small Bingham number, Bn = 1/36, at which stresses induced by density variation are strong enough and the viscoplastic layer cannot be entirely unyielded. The interplay between stresses induced by surface tension and density variation results in various regimes with up to 5 yielded and unyielded regions. The configuration presented in Fig. 2a is typical for any Bn < 1/16. In Fig. 2b, Bn = 1/16. Here 5-layer regime is not possible, as well as for higher values of the Bingham number, and the domains corresponding to 4-layer flow shrink. Figure 2c corresponds to the case Bn = 1/8. A region corresponding to entirely unyielded Herschel-Bulkley fluid (1b, marked grey) is evident. This configuration is typical for 1/16 < Bn < 1/4. In Fig 2(d) Bn = 1/2. One can observe that the regions of 4 and 5 layer regimes disappear, and that corresponding to an entirely unyielded plastic is extended. The configuration is typical for high values of the Bingham number, Bn > 1/4, i.e. for cases when Marangoni convection dominates over the natural convection, e.g. under microgravity conditions.

As soon as the stress distribution is known, the velocity field in the Herschel-Bulkley layer can be obtained by integrating equations (21) with no-slip condition at the bottom, y = – 1, which results in the expressions

$$V_{HB}(y) = \int_{-1}^{y} \mathrm{sign}\,[\tau_{HB}(\eta)]\,\{\max\,[|\tau_{HB}(\eta)| - Bn, 0]\}^{1/n} d\eta, \quad y \in (-1,0). \tag{31}$$

Several typical graphs of velocity in viscoplastic layer versus y are presented in Fig 3 for n=1 (Bingham fluid). In Figs. 3 (a)-(d) Bn = 0.02 < 1/16. For such small values of Bingham number, various multilayer regimes of the flow are possible. Each of these figures illustrates the change of the regime with the relative magnitude of Marangoni traction, M, for fixed value of the parameter B.

In Figure 3 (a) B= –0.4, M= 0.28, 0.044 and 0.06 for dashed, solid and dashed-dotted curves, respectively. One can see that with the growth of the Marangoni traction in the positive direction the four-layer pattern (dashed line) changes to a 5-layer (solid line) and then to a 3-layer (dashed-dotted) one.

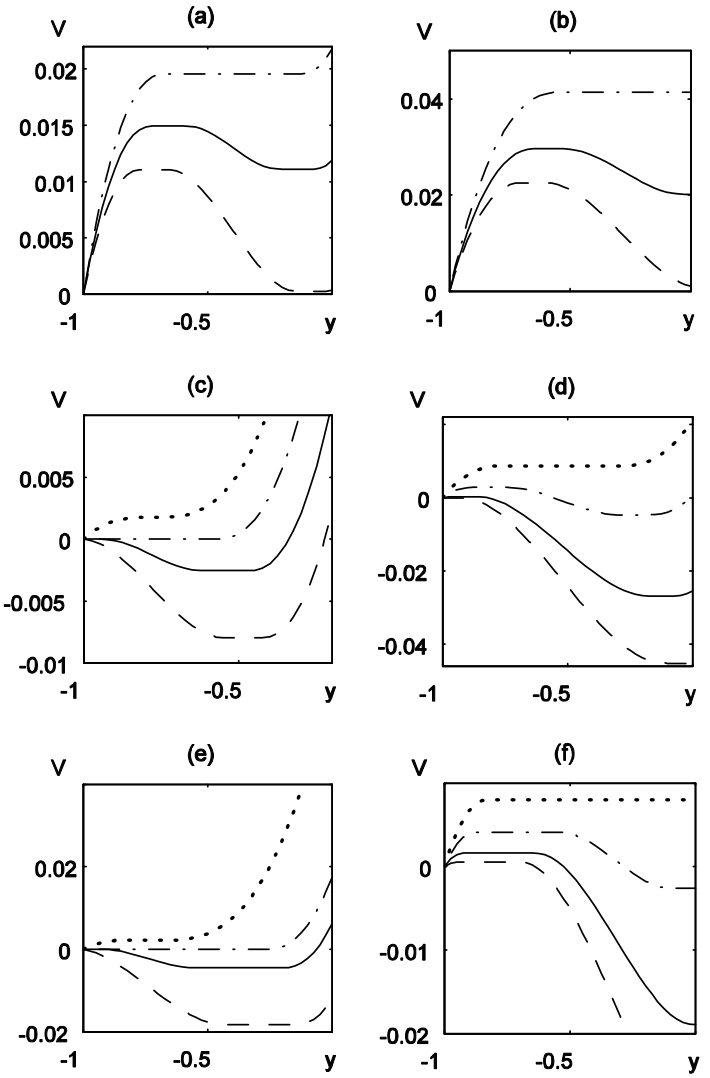

Figure 3: Velocity profiles in viscoplastic fluid for various values of parameters. (a) Bn = 0.02, $B = -0.4$, M = 0.28, 0.044 and 0.06 for dashed, solid and dashed-dotted curves, respectively; (b) Bn = 0.02, B = – 0.28, M = – 0.032, – 0.01 and 0.002, for dashed, solid and dashed-dotted curves, respectively; (c) Bn = 0.02, B= – 0.78, M= 0.258, 0.272, 0.3 and 0.324 for dashed, solid, dashed-dotted and dotted curves, respectively; (d) Bn = 0.02, B= – 0.52, M = 0.032, 0.056, 0.09 and 0.124 for dashed, solid, dashed-dotted and dotted curves, respectively, (e) Bn = 0.068, B= – 0.74, M= 0.16, 0.188, 0.22 and 0.338 for dashed, solid, dashed-dotted and dotted curves, respectively; (f) Bn = 0.068, B = – 0.32, M = – 0.086, – 0.066, – 0.04 and –0.012 for dashed, solid, dashed-dotted and dotted curves, respectively.

In Figure 3 (b) the magnitude of the parameter B is smaller, $B = -0.28$, $M = -0.032$, -0.01 and 0.002, for dashed, solid and dashed-dotted curves, respectively. In this case, the 3-layer pattern (dashed line) changes to a 4-layer (solid line) and then to a 2-layer (dashed-dotted) ones.

In Figure 3 (c) $B = -0.78$. At $M = 0.258$ (dashed line) the Marangoni traction is relatively weak, and the negative direction of the flow is determined by natural convection. Three-layer regime is evident. At $M = 0.272$ (solid curve) the traction in positive direction is higher. The fluid near the bottom is unyielded, then flows in the negative direction, then follow a second quasi-solid region, and a yielded layer with changing flow direction. At $M = 0.3$ (dashed-dotted line) the region of the flow with negative velocity disappears and a 2-layer regime with unyielded lower region is observed. At $M = 0.324$ (dotted curve), the fluid near the bottom is again yielded, but the velocity is positive.

In Figure 3 (d) $B = -0.52$. At $M = 0.032$ (dashed line) quasi-solid regions are presented near the bottom and near the interface while in the middle the fluid is yielded and flows in the negative direction. At $M = 0.056$ (solid curve) a second yielded region appears near the interface. At $M = 0.09$ (dashed-dotted line) a 5 layer pattern takes place and at $M = 0.124$ (dotted curve) a yielded region in the middle disappears and a 3b regime is observed.

In Figs. 3 (e) and 3 (f) the Bingham number is higher $Bn = 0.068 > 1/16$ and a 5 layer regime is not possible. In Figure 3 (e) $B = -0.74$. The flow pattern changes from a 3-layer flow in the negative direction at $M = 0.16$ (dashed line) to a 4 layers at $M = 0.188$ (solid curve), then to two layers with unyielded fluid near the bottom at $M = 0.22$ (dashed-dotted line) and, finally, to a 3 layer regime with flow in the positive direction at $M = 0.338$ (dotted curve).

In Figure 3 (f) $B = -0.32$. The flow pattern changes from a 2-layer flow with unyielded fluid near the bottom at $M = -0.086$ (dashed line) to a 3-layer regime $M = -0.066$ (solid curve), then to a 4-layer pattern at $M = -0.04$ (dashed-dotted line) and to 2 layers with an unyielded one near the interface at $M = -0.012$ (dotted curve).

4 Free boundary flow

Assume a free upper boundary. It follows immediately from (27), that

$$B = \delta d, \quad M = Ma_N + Ma_{HB} + B_N d - \frac{\delta}{2} d^2 = Ma_N + Ma_{HB} + \frac{\delta}{2} d^2 \tag{32}$$

and, thus, the stress distribution is given explicitly by (30). Note that regimes with more than 3 layers are possible only if $B < 0$ and, hence, $\delta < 0$, i.e. when the

combined effect of temperature and concentration variation on the density of the upper layer is negative (the density of the Newtonian fluid decreases with x).

As soon as the stress distribution is known, the velocity field can be obtained by integrating equations (21) with a no-slip condition at the bottom, $y = -1$, and continuity at the interface, $y = 0$, which results in the expressions

$$\begin{aligned} V_{HB}(\xi) &= \int_{-1}^{\xi} \mathrm{sign}\left[\tau_{HB}(\eta)\right]\left\{\max\left[|\tau_{HB}(\eta)| - Bn, 0\right]\right\}^{1/n} d\eta, \quad \xi \in (-1,0), \\ V_N(\xi) &= \int_{-1}^{0} \mathrm{sign}\left[\tau_{HB}(\eta)\right]\left\{\max\left[|\tau_{HB}(\eta)| - Bn, 0\right]\right\}^{1/n} d\eta + d\int_{0}^{\xi} \tau_N(\eta) d\eta \\ &= V_{HB}(0) + \frac{\delta d^3}{6\mu}\xi^3 - \frac{Bd^2}{2\mu}\xi^2 + \frac{(M - Ma_{HB})\,d}{\mu}\xi \\ &= V_{HB}(0) + \frac{Ma_N d}{\mu}\xi + \frac{\delta d^3}{2\mu}\left(\frac{\xi^3}{3} - \xi^2 + \xi\right) \\ &= V_{HB}(0) + \beta\xi + \frac{\gamma}{2}\left(\frac{\xi^3}{3} - \xi^2 + \xi\right), \quad \xi \in (0,1). \end{aligned} \tag{33}$$

where $\xi = y$ for $y < 0$ and $\xi = y/d$ for $y \geq 0$. Note that, while V_N is a simple polynomial of the vertical coordinate, integration of (33) in elementary functions is possible for the special case of a Bingham fluid, e.g., $n = 1$, in which case $V_{HB}$is a piecewise polynomial function. Explicit expressions in this case are given in the Appendix.

It is evident from (33) that, while the velocity in the viscoplastic domain is a function of parameters *M, B, Bn* and n solely, that in the Newtonian liquid depends on 3 additional parameters, $\beta = Ma_N d/\mu, \gamma = \delta d^3/\mu$ and d. The dependence of velocity profile on the parameter d is solely through the stretched coordinate ξ. The effect of the parameters β, γ, n and *Bn* is illustrated in Fig. 4, where the velocity in both phases is plotted versus the spatial coordinate ξ.

In Fig. 4a, $Bn = 0.02$, $B = -0.4$, $M = 0.044$, $\beta = 0.02, \gamma = -0.1$ and n= 0.8, 1 and 1.2 for dashed, solid and dashed-dotted curves, respectively. A strong influence of the power law index is evident. Note that this parameter affects the motion in the Newtonian fluid solely through the change of the velocity at the interface. Thus the curves in the Newtonian region $\xi > 0$ are parallel.

Figure 4b illustrates the effect of the Bingham number on the velocity profile. Here $B = -0.4$, $M = -0.044$, n= 1, $\beta = 0.02$ and $\gamma = -0.1$. Dashed-dotted line is computed for $Bn = 0.05$. A two-layer regime of the flow of the Herschel-Bulkley

fluid is evident. For lower values of the yield stress at Bn = 0.015 (solid curve) and Bn = 0.005 (dashed curve) one can observe a 5 layer and an entirely yielded flows. The dependence of velocity on the Bingham number, in contrast to all the other parameters, is not always monotonic. See the intersection of solid and dashed dotted curves. Similar to Fig 4a, the curves in the Newtonian region $\xi > 0$ are parallel, since the Bingham number does not enter the equations governing the motion of Newtonian fluid and, thus, affects its motion solely through the change of the velocity at the interface.

Figures 4c and 4d demonstrate the influence of the parameters β and γ. These have no effect on the flow of the viscoplastic medium. Thus, a single curve is seen at $\xi < 0$ and all the curves corresponding to the Newtonian fluid intersect at $\xi = 0$.

When the velocity is known, the temperature and concentration distributions are determined by integrating equations (22) with boundary and interfacial conditions (25)-(27), which results in:

$$\Theta_{HB}(y) = \kappa \left(q_T - Pe_N^T \int_0^d V(\eta) d\eta \right) (y+1) - Pe_{HB}^T \int_{-1}^0 [1 + \min(y,\eta)] V(\eta) d\eta,$$

$$\begin{aligned} \Theta_N(y) =& \kappa \left(q_T - Pe_N^T \int_0^d V(\eta) d\eta \right) + q_T y \\ & - Pe_{HB}^T \int_{-1}^0 (1+\eta) V(\eta) d\eta - Pe_N^T \int_0^y \min(y,\eta) V(\eta) d\eta, \end{aligned} \tag{34}$$

$$\begin{aligned} \Phi_{HB}(y) =& \frac{D_N}{D_{HB}} \left(q_C - \frac{D_N^T T^*}{D_N C^*} q_T + Pe_N^C \int_0^d V(\eta) d\eta - \frac{D_{HB}^T T^*}{D_{HB} C^*} \Theta'_{HB}(0) \right. \\ & \left. + \frac{D_N^T T^*}{D_{HB} C^*} \Theta'_N(0) \right) (y+1) - Pe_{HB}^C \int_{-1}^0 [1 + \min(y,\eta)] V(\eta) d\eta, \end{aligned} \tag{35}$$

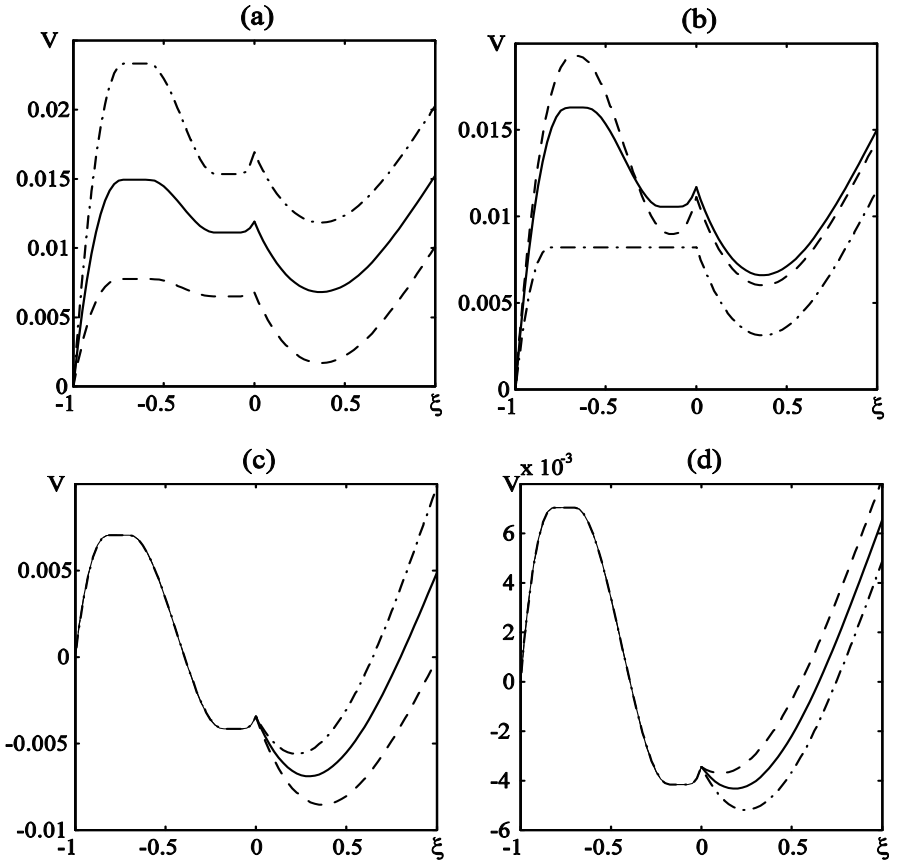

Figure 4: Velocity profiles in Herschel-Bulkley and Newtonian fluids for free boundary flow. (a) Bn = 0.02, B = – 0.4, M = 0.044, $\beta = 0.02, \gamma = -0.1$, n= 0.8, 1 and 1.2 for dashed, solid and dashed-dotted curves, respectively; (b) B = – 0.4, M = – 0.044, n= 1, $\beta = 0.02, \gamma = -0.1$,$Bn$ = 0.005, 0.015 and 0.05 for dashed, solid and dashed-dotted lines, respectively; (c) Bn = 0.02, B= – 0.44, M= 0.044, n = 1, $\gamma = -0.1, \beta = 0.02, 0.025$ and 0.03 for dashed, solid and dashed-dotted curves, respectively; (d) Bn = 0.02, B= – 0.44, M = 0.044, n = 1, $\beta = 0.02, \gamma = -0.05, -0.06$ and – 0.07 for dashed, solid and dashed-dotted lines, respectively.

$$\Phi_N(y) =$$

$$\frac{D_N}{\alpha_{eq} D_{HB}} \left(q_C - \frac{D_N^T T^*}{D_N C^*} q_T + Pe_N^C \int_0^d V(\eta) d\eta - \frac{D_{HB}^T T^*}{D_{HB} C^*} \Theta'_{HB}(0) + \frac{D_N^T T^*}{D_{HB} C^*} \Theta'_N(0) \right)$$

$$+ \left(q_C - \frac{D_N^T T^*}{D_N C^*} q_T \right) y - Pe_{HB}^C \int_{-1}^{0} (1+\eta) V(\eta) d\eta - Pe_N^C \int_0^y \min(y, \eta) V(\eta) d\eta. \tag{36}$$

If the temperature/concentration distribution is specified on the upper boundary instead of the corresponding flux, in the above formulae

$$q_T = \left(\Theta_1 + Pe_N^T \int_0^d (k-\eta) V(\eta) d\eta + Pe_{HB}^T \int_{-1}^0 (1+\eta) V(\eta) d\eta \right) / (\kappa + d),$$

$$q_C = \left(\Phi_1 + Pe_N^C \int_0^d (k-\eta) V(\eta) d\eta + Pe_{HB}^C \int_{-1}^0 (1+\eta) V(\eta) d\eta \right) / (\kappa + d)$$

the explicit expressions for the temperature profile in the case of Bingham fluid with various types of boundary conditions are given in the Appendix.

The results for the temperature field corresponding to zero flux condition at the upper boundary and to the velocity profiles presented in Fig. 4 are given in Fig. 5. In Fig. 5a, Bn = 0.02, B = – 0.4, M = 0.044, $\beta = 0.02, \gamma = -0.1$ and n= 0.8, 1 and 1.2 for dashed, solid and dashed-dotted curves, respectively. The velocity is positive (see Fig 4a), hence, the temperature is convex and temperature deviation is negative everywhere. The magnitude of temperature deviation increases with the velocity.

Figure 5b illustrated the effect of the Bingham number on the temperature profile. Here B = – 0.4, M = – 0.044, n= 1, $\beta = 0.02$ and $\gamma = -0.1$. Solid, dashed and dashed-dotted lines are computed for Bn = 0.0015, 0.005 and 0.05, respectively. One can see that the curves computed for low Bingham numbers almost coincide, though the velocity profiles are essentially different. At higher Bn, the velocity and the temperature deviation magnitudes are considerably smaller.

Figures 5c and 5d demonstrate the influence of the parameters β and γ that have no influence on the flow of the viscoplastic medium (see Figs. 4c and 4d). However, the effect on the temperature distribution is evident. In contrast to the cases presented in Figs 5a and 5b, here the flow changes its direction and the temperature profiles are not monotonic, but exhibit several maxima and minima.

For all the examples we chose a heat insulated upper boundary, $q_T = 0$, and equal thermal properties for the two fluids, Pe=1 and $\kappa = 1$. If $q_T \neq 0$ an appropriate linear function should be added to the temperatures calculated for zero heat flux. Different thermal conductivities result in a jump of $d\Theta/dy$ at the interface. Due to the similarity of the equations for the temperature and concentration the latter is proportional to Θ (for homogeneous boundary conditions) and we do not present its distribution separately. However it is worth noting that while the Peclet number for the temperature is positive, in the presence of the Soret effect, the combined Peclet number for the concentration, see (23), can be negative as well and result in a negative proportionally coefficient between the temperature and concentration.

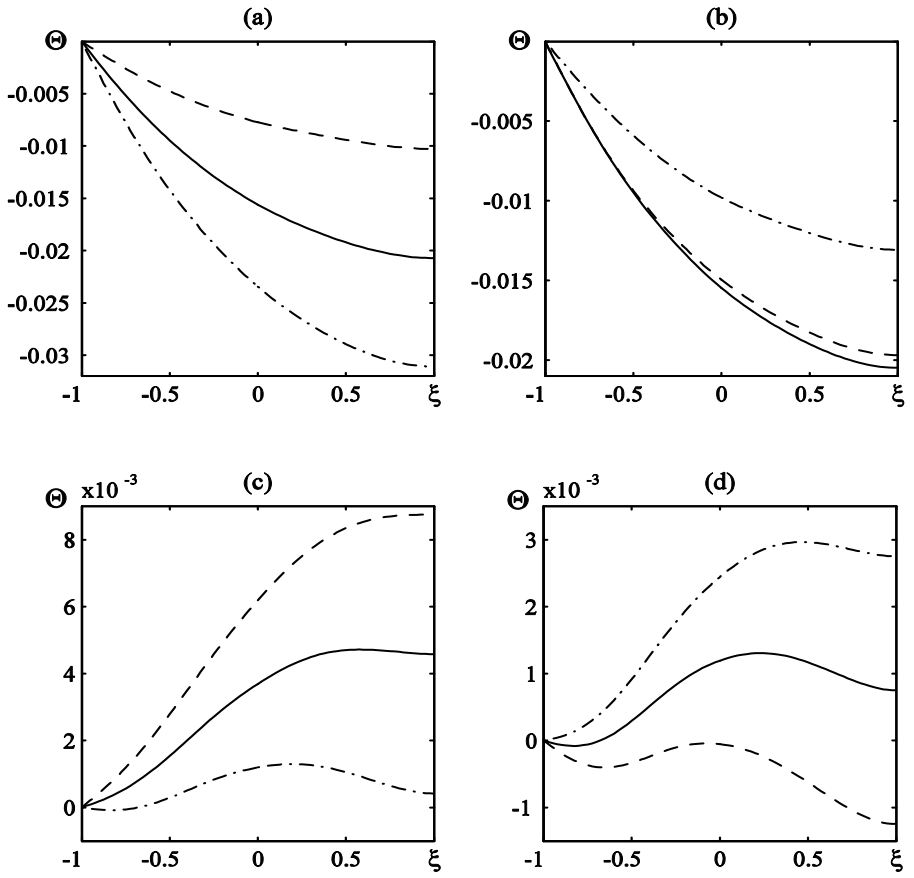

Figure 5: Temperature profiles in Herschel-Bulkley and Newtonian fluids for $q_T = 0$, $\kappa = 1$, Pe = 1 and various values of other parameters. (a) Bn = 0.02, B = – 0.4, M = 0.044, $\beta = 0.02, \gamma = -0.1$, n= 0.8, 1 and 1.2 for dashed, solid and dashed-dotted curves, respectively; (b) B = – 0.4, M = – 0.044, n= 1, $\beta = 0.02, \gamma = -0.1$,$Bn$ = 0.005, 0.0015 and 0.05 for dashed, solid and dashed-dotted lines, respectively; (c) Bn = 0.02, B= – 0.44, M= 0.044, n = 1, $\gamma = -0.1, \beta = 0.02, 0.025$ and 0.03 for dashed, solid and dashed-dotted curves, respectively; (d) Bn = 0.02, B= – 0.44, M = 0.044, n = 1, $\beta = 0.02, \gamma = -0.05, -0.06$ and – 0.07 for dashed, solid and dashed-dotted lines, respectively.

A popular approximation employed by most of previous works on Birikh solutions for the Newtonian is that of non-deformable interfaces, which normal stress balance at free boundary and interfaces. The misbalance in the boundary conditions at

the flat interfaces results naturally in its deformations. The non-deformable interface approximation is consistent with the case of very large surface tension (small capillary number) providing that the induced deformations remain negligibly small. In this paper we concentrate on exact solutions satisfying all the boundary conditions. A brief discussion on possible modification of these solutions to the case of non-deformable interfaces is given below.

Neglecting the normal stress balance leaves 2 parameters, B_{HB} and B_N, free. Choosing these parameters allows to prescribe the fluxes of the both fluids. Normally, these fluxes are chosen to be zero, to model the flow in a container of finite extension.

The fluxes of each phase are

$$\begin{aligned} Q_{HB} &= \int_{-1}^{0} V_{HB}(y)dy = \int_{-1}^{0} y\,\mathrm{sign}\left[\tau_{HB}(y)\right]\left\{\max\left[|\tau_{HB}(y)| - Bn, 0\right]\right\}^{1/n} dy, \\ Q_N &= d\int_{0}^{1} V_{HB}(\xi)d\xi = -\frac{5\delta d^4}{12\mu} + \frac{B_N d^3}{3\mu} + \frac{Ma_N d^2}{2\mu} + V_{HB}(0)d \end{aligned} \tag{37}$$

Note that Q_{HB} is a function of parameters M,B_{HB}, Bn and n solely,

$$Q_{HB} = Q_{HB}(M, B_{HB}, Bn, n).$$

Hence, the parameter B_{HB} can be determined specifying the flux of the Herschel-Bulkley fluid. The flux of Newtonian fluid, Q_N, depends on 3 additional parameters d, μ and Ma_N, $Q_N = Q_N(M, B_{HB}, Bn, n, d, \mu, Ma_N, B_N)$. When Q_N is known B_N is found from (3) explicitly. An interesting case of zero flux of the Herschel-Bulkley fluid modeling the flow in a finite length container (far from the lateral boundaries) corresponds, for given values of Bn and n, to the curve

$$Q_{HB}(M, B_{HB}, Bn, n) = 0, \tag{38}$$

in the (B_{HB}, M) plane. Examples of such curved are presented in Fig. 2 (dashed lines, B=B_{HB}).

If the Herschel-Bulkley fluid is entirely unyielded, it does not flow and has a zero flux. Hence equation (38) is satisfied by any (M, B_{HB}) corresponding to the regime 1b (see Fig 2). Thus for $Bn > 1/4$, $0 < B < 2Bn - 1/2$, any $M \in (Bn,\ Bn - B_{HB} - 1/2)$ satisfies (38). Similarly, in the case $Bn > 1/4$, and $-2Bn - 1/2 < B_{HB} < 0$, the solution is $M \in (\max(B_{HB}^2/2 - Bn,\ -Bn - B_{HB} - 1/2),\ \min(Bn, Bn - B_{HB} - 1/2))$, while for any pair $B_{HB} \in (-2\sqrt{Bn}, -1 + 2\sqrt{Bn})$, $M \in (B_{HB}^2/2 - Bn,\ \min(Bn, Bn -$

$B_{HB} - 1/2)$) satisfies (38) if 1/16 < *Bn* < 1/4. If $Bn \leq 1/16$ or 1/16 < *Bn* < 1/4 and $B_{HB} \notin (-2\sqrt{Bn}, -1 + 2\sqrt{Bn})$ or *Bn* > 1/4 and $B_{HB} \notin (-2Bn - 1/2, 2Bn - 1/2)$, equation (38) has a unique solution $M(Bn,n,B_{HB})$. Examples of sets defined by (38) are presented in Fig 2 for n = 1 (dashed lines) and n = 0.25 (dashed-dotted curves). Any point of domains marked by grey, belongs to this set as well.

It is easy to see that for a given *Bn*, the curves $Q_{HB}(Bn,n,M,B_{HB}) = 0$ intersect at the point (B_{HB} = 0, *M*= – 1/4). For a free boundary flow, B_{HB} = 0 correspond to a special case of the absence of natural convection in the upper layer (i.e. a single layer flow and the case when the upper layer has constant density).

Note that not all the flow regimes described in section 2 are compatible with the zero flux condition, which requires that velocity is either identically zero or it changes sign. Since the velocity vanished at the bottom, the stress should change sign as well, hence zero flux is possible only for 3, 4 and 5-layer regimes.

5 Flow between two solid walls.

When the system is bounded from above by a solid wall instead of free boundary, the first two conditions (26) are replaced by the no-slip condition $V(d)$=0 and by specifying the total flux in the lower layer, Q_{HB}. This flux can be fixed arbitrary, but in this paper we concentrate on the case $Q_{HB} = 0$, that corresponds to the modeling of the flow in the container with final horizontal extension. In this case the parameter M and B that govern the flow regime in the viscoplastic medium cannot be determined independently from the velocity field, but should be obtained by solving equations

$$Q_{HB}(Bn,n,M,B) = 0, \tag{39}$$

$$V_{y=d}(Bn,n,Ma_{HB},\mu,\delta,d,M,B) = 0, \tag{40}$$

with respect to M and B.

The effect of the parameters δ, μ, d and Ma_{HB} on the flow pattern is illustrated in Fig. 6, where the velocity in both phases is plotted versus the spatial coordinate ξ. All the curves are computed for n= 1, *Bn* = 1/36. For a given velocity field, the temperature distribution is given by (14). Temperature distributions corresponding to velocity fields presented in Fig 6 are illustrated in Fig 7. Solid lines are computed for δ= – 1, d = 1, μ= 20 and Ma_{HB}= 0.3. This choice of parameters corresponds to a 5-layer flow regime for the Herschel-Bulkley fluid. As in the previous section we chose a heat insulated upper boundary, $q_T = 0$, and equal thermal properties of the two fluids, *Pe*=1 and $\kappa = 1$. The effect of these parameters is similar to that discussed in section 4. The deviation of concentration is proportional to the

deviation of temperature, with the proportionality coefficient that can be negative (see the discussion in section 4).

In Figs. 6a and 7a, $\delta = -1$, $d = 1$, $\mu = 20$ and $Ma_{HB} = 0$, 0.16 and 0.3 for dashed-dotted, solid and dashed lines, respectively. Dashed-dotted lines correspond to the flow induced by natural convection solely. The Newtonian fluid flows in negative direction. The velocity in this layer is a monotonically increasing function of y. With the growth of the Marangoni traction, the velocity near the interface increases. At $Ma_{HB} = 0.16$ (dashed curve), flow in different directions is observed and the velocity profile exhibits internal minimum and maximum. At higher Marangoni traction $Ma_{HB} = 0.3$ (solid line), the Newtonian fluid flows in positive direction, with the velocity monotonically decreasing with y. For the range of parameters presented in Fig 6a, the velocity of the Herschel-Bulkley fluid decreases near the bottom and increases near the interface. The corresponding temperature profiles computed with heat insulated upper boundary presented in Fig.7a change from positive monotonically increasing (dashed-dotted line) to positive with an internal maximum (dashed curve) and, finally, to a monotonically decreasing negative one (solid line).

Figures. 6b and 7b illustrate the effect of the Newtonian fluid viscosity on the flow and heat transfer. Here, $\delta = -1$, $d = 1$ and $Ma_{HB} = 0.3$. $\mu = 2$ and 20 for dashed and solid lines, respectively. Dashed-dotted line presents a limit $\mu \to \infty$. In the latter case, the Newtonian fluid is almost quiescent, and a 5-layer flow is evident in the Herschel-Bulkley medium. The corresponding temperature deviation grows in the viscoplastic layer and almost does not change in the Newtonian region. At relatively high viscosity, $\mu = 20$ (solid line), the Newtonian fluid flows in the positive direction and the velocity monotonically decreases with y. The corresponding temperature deviation profile is negative. At lower viscosity, $\mu = 2$ (dashed line), the velocity profile in the upper layer is not monotonic, and a region of flow in the negative direction is evident. The corresponding temperature deviation profile exhibits several alternating concave and convex regions. The velocity in the lower layer grows with μ near the bottom and decays near the interface.

Figures 6c and 7c demonstrate the influence of the parameter δ that characterizes the natural convection in the Newtonian fluid. Here $d = 1$, $\mu = 20$ and $Ma_{HB} = 0.3$. In the case when the natural convection in the upper layer is absent, $\delta = 0$ (dashed line), the velocity profile in the upper layer is a quadratic parabola (Couette – Poiseuille flow). At $\delta = -1$ (solid curve), the velocity in the upper layer changes its direction and regions of convex and concave profile are evident. At $\delta = 1$ (dashed-dotted curve), the density in the upper layer grows with x, in contrast to all the other examples described so far. Here a 4-layer flow regime in the Herschel-Bulkley fluid is observed. The velocity profile in the upper layer has a convex shape. The temperature deviation profiles change from negative corresponding mostly to positive

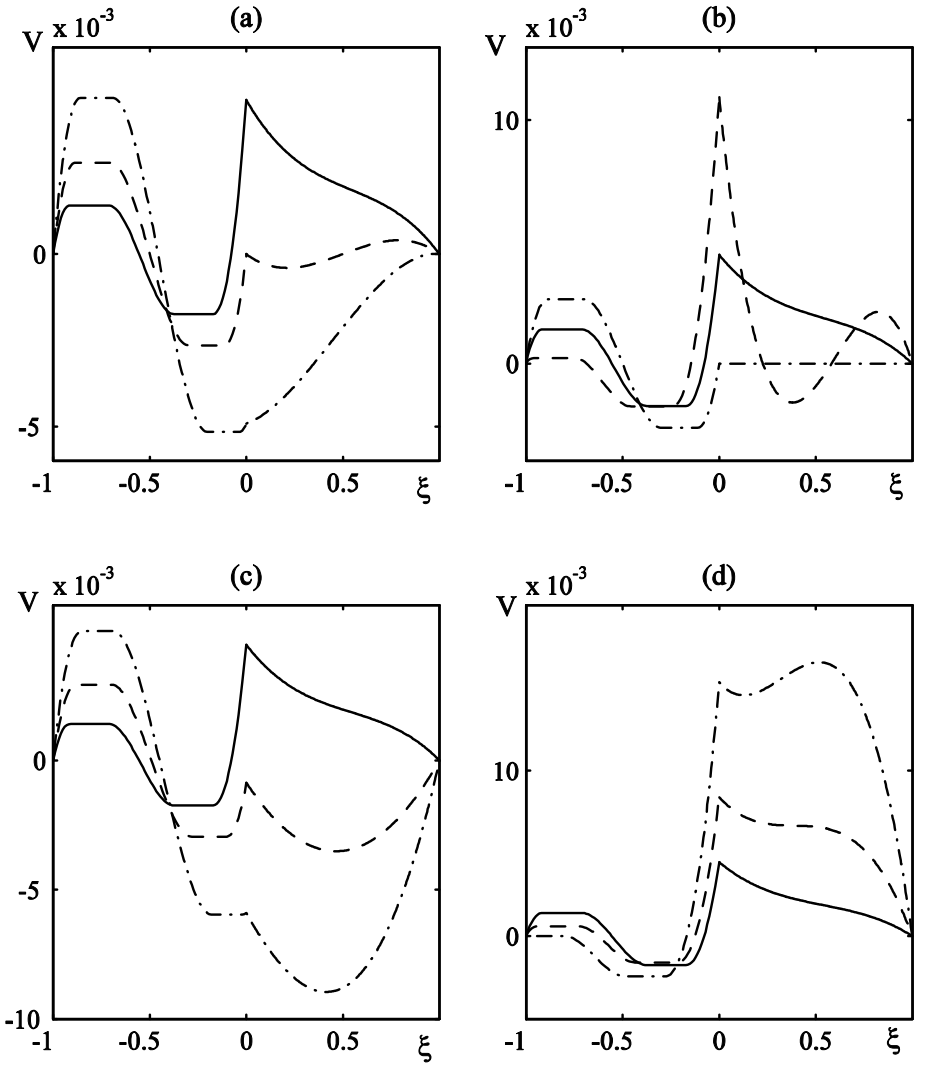

Figure 6: Velocity profiles in Herschel-Bulkley and Newtonian fluids for the flow between two solid walls: (a) $\delta = -1$, $d = 1$, $\mu = 20$, $Ma_{HB} = 0.16$, 0.3 and 0 for dashed, solid and dashed-dotted lines, respectively. (b) $\delta = -1$, $d = 1$, $Ma_{HB} = 0.3$. Dashed, solid and dashed-dotted curves are computed for $\mu = 2$, 20 and $\mu \to \infty$, respectively; (c) $d = 1$, $\mu = 20$, $Ma_{HB} = 0.3$, $\delta = -1$, 1 and 0 for solid, dashed-dotted and dashed lines, respectively; (d) $\delta = -1$, $\mu = 20$, $Ma_{HB} = 0.3$, $d = 1.5$, 2 and 1 for dashed, dashed-dotted and solid curves, respectively.

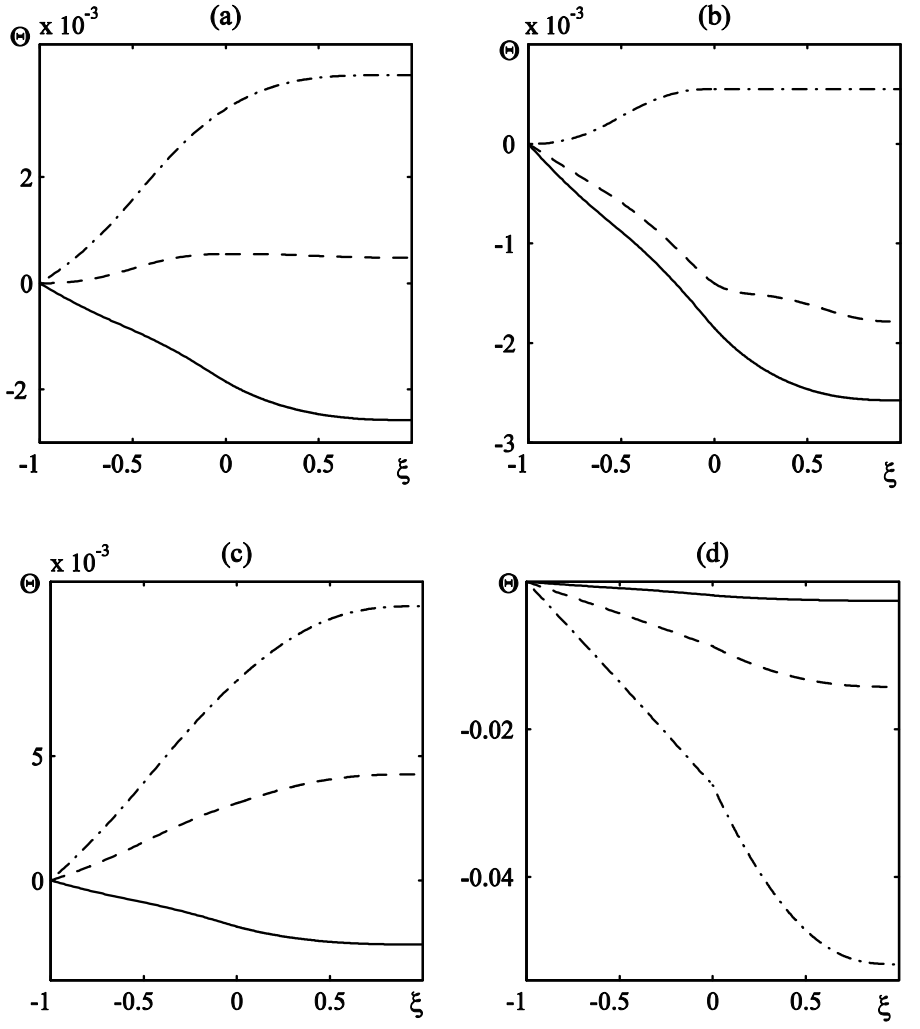

Figure 7: Temperature profiles in Herschel-Bulkley and Newtonian fluids for the flow between two solid walls: (a) $\delta = -1$, $d = 1$, $\mu = 20$, $Ma_{HB} = 0.16$, 0.3 and 0 for dashed, solid and dashed-dotted lines, respectively; (b) $\delta = -1$, $d = 1$, $Ma_{HB} = 0.3$. Dashed, solid and dashed-dotted curves are computed for $\mu = 2$, 20 and $\mu \to \infty$, respectively; (c) $d = 1$, $\mu = 20$, $Ma_{HB} = 0.3$, $\delta = -1$, 1 and 0 solid, dashed-dotted and dashed lines, respectively; (d) $\delta = -1$, $\mu = 20$, $Ma_{HB} = 0.3$, $d = 1.5$, 2 and 1 for dashed, dashed-dotted and solid curves, respectively.

velocity at $\delta = -1$ (solid line), to positive concave shapes for mostly negative velocity (dashed and dashed dotted lines).

Figures 6d and 7d illustrate the influence of the Newtonian layer width. $\delta = -1$, $\mu = 20$, $Ma_{HB} = 0.3$ and $d = 1$, 1.5 and 2 for solid, dashed and dashed-dotted lines, respectively. One can observe a strong retardation effect of the upper wall at small d (solid line). In this case the flow in the Newtonian layer is weak and has an almost linear profile. With the increase of d, the retardation becomes weaker. The flow in the Newtonian fluid is intensified, together with the velocity in the viscoplastic medium near the interface. In contrast to this, the velocity near the bottom decreases with the growth of the upper layer width, and at $d = 2$ one can observe an unyielded quiescent region adjacent to the bottom. The temperature deviation in these cases is negative.

6 Conclusions and discussion

A variety of exact analytical solutions describing natural and thermocapillary convection in a horizontal double layer system consisting of a Newtonian and Herschel-Bulkley fluids subjected to longitudinal temperature and concentration gradients is constructed. The velocity is directed horizontally and depends on a vertical coordinate, y, while the temperature and concentration fields are the sums of linear functions of horizontal coordinate, x, and non-linear functions of y. This type of solutions that was first found by Birikh (1966), is widely used to model thermocapillary flows in single and multi-layer configurations. Birikh (1966) and most of subsequent studies employed this solution to model experiments, where the flow takes place in a container of finite extension, requiring zero flux condition. Recently, Goncharova and Kabov (2009) constructed Birikh type solutions satisfying all exact conditions at the interfaces between liquid and co-current gas flow and demonstrated that the gas flow can be used to control convection in liquid. In this work we follow the approach of Goncharova and Kabov (2009).

The lower boundary of the system is a solid wall with no-slip, while the upper one if either a solid wall or a free surface. It was demonstrated that, depending on the governing parameters of the system, viscoplastic layer is entirely yielded or unyielded, or it can be yielded partially, exhibiting up to 5 flowing and quasi-solid layers. The dependence of the flow patterns (appearance and position of unyielded regions), velocity profile, mass and heat transfer rate on the governing parameters have been studied. Regimes with partial yielding and unyielded regions located near the interface are of special interest. As was demonstrated by Frigaard (2001) and Moyers-Gonzalez, Frigaard, and Nouar (2004), in a somewhat similar isothermal flow, such configurations can suppress interfacial instability and result in a super-stable flow.

In this work all the physical parameters of the media, except for the interfacial tension and density, are assumed temperature and concentration independent. However, the rheological characteristics of many viscoplastic fluids exhibit strong dependence on the temperature and on the concentration of some chemical species. The constructed solutions can be generalized to the case of, say, concentration dependent parameters, if the flow is induced by a longitudal temperature gradient, concentration being a function of vertical coordinate solely. We plan to study such solutions in our future work.

Acknowledgement: This research was supported by The Israel Science Foundation (grant 847/06). OML acknowledge the support of the Ministry of Immigrant Absoption.

References

Bingham, E. C. (1922): *Fluidity and Plasticity*. Mc.Graw-Hill, New York.

Birikh R. V. (1966): Thermocapillary convection in a horizontal layer of liquid. *J. Appl. Mech. Techn. Physics*, vol. 7 pp. 43-46.

Bhavaraju, S. M.; Mashelkar, R. A.; Blanch, H. W. (1978): Bubble motion and mass transfer in non-Newtonian fluids. *AIChE J.*, vol. 24, pp. 1063-1070.

Burgos, G. R.; Alexandrou, A. N.; Entov, V. (1999): On determination of yield surfaces in Herschel-Bulkley fluids. *J. Non-Newtonian Fluid Mech.*, vol. 43, pp. 463-483.

Cherkasov, S. G. (1979): Combined convection of viscoplastic liquid in a plane vertical layer, *Fluid Dynamics*, vol. 15, pp. 111-113.

Dubash, N.; Frigaard, I. (2004): Conditions for static bubbles in viscoplastic fluid. *Phys. Fluids*, vol. 16, pp. 4319-4330.

Dubash, N.; Frigaard, I. (2007): Propagation and stopping of air bubbles in Carbopol solutions. *J. Non-Newtonian Fluid Mech.*, vol. 142, pp. 123–134.

Frigaard, I. A. (2001): Super-stable parallel flows of multiple visco-plastic fluids, *J. Non-Newtonian Fluid Mech.*, vol. 100, pp. 49–76.

Goncharova, O.; Kabov, O. (2009): Gas flow and thermocapillary effects on fluid flow dynamics in a horizontal layer. Microgravity Sci. Technol. vol. 21, pp.129-137.

Huen, C. K.; Frigaard, I. A.; Martinez, D. M. (2007): Experimental studies of multi-layer flows using a visco-plastic lubricant *J. Non-Newtonian Fluid Mech.*, vol. 142, pp. 159-161.

Li J.; Renardy Y. Y. (2000): Shear-induced rupturing of a viscous drop in a Bing-

ham liquid. *J. Non-Newtonian Fluid Mech.*, vol. 95, pp. 235-251.

Lyubimova, T.P.; Lyubimov, V.D. (1980): Stationary convection of viscoplastic fluid in a vertical layer. *Fluid Dynamics*, vol. 16, pp. 118-123.

Metivier, C; Nouar, C. (2008): On linear stability of Rayleigh – Benard - Poiseuille flow of viscoplastic fluids. *Phys. Fluids*, vol. 20, pp 104101.

Moyers-Gonzalez, M.A.; Frigaard, I.A.; Nouar, C. (2004): Nonlinear stability of a visco-plastically lubricated viscous shear flow. *J. Fluid Mech.*, vol. 506, pp. 117–146.

Napolitano, L.G. (1980): Plane Marangoni-Poiseuille flow of two immiscible fluids. *Acta Astronautica*, vol. 7, pp. 461-478.

Nouar C. (2005): Thermal convection for a thermo-dependent yield stress fluid in an axi-symmetric horizontal duct. *Int. J. Heat Mass Transfer* vol. 48, 5520-5535

Oldroyd, J. D. (1947a): A rational formulation of the equations of plastic flow for a Bingham solid. *Proc. Camb. Phil. Soc.*, vol. 43, pp. 100-105.

Oldroyd, J. D. (1947b): Two-dimensional plastic flow of a Bingham solid. *Proc. Camb. Phil. Soc.*, vol. 43, pp. 383-395.

Potapov, A.; Spivak, R.; Lavrenteva, O. M.; Nir, A. (2006): Motion and deformation of drops in Bingham fluid. *Ind. Eng. Chem. Res.*, vol. 45, pp. 6985-6995

Prager, W. (1954): On slow viscoplastic flow. In *Studies in Mathematics and Mechanics: R. von Mises presentation volume*, pp. 208 – 216. Academic press.

Pukhnachov, **V.V.** (2000): Group-theoretical nature of the Birikh solution and its generalizations. Book of Proc. *Symmetry and differential equations*, Krasnoyarsk, pp. 180-183 (in Russian).

Singh, J.P.; Denn, M. M. (2008): Interacting two-dimensional bubbles and droplets in yield stress fluid. *Phys. Fluids*, vol. 20, pp. 040901-1 – 040901-11.

Stein, S.; Buggisch, H. (2000): Rise of pulsating bubbles in fluids with a yield stress. *Z. Angew. Math. Mech.*, vol. 80, pp. 827-834.

Vasil'chenko, S.V.; Potapov, A.G. (1996): Gas bubble dynamics in a viscoelastocplastic medium. *Heat Transfer Res.*, vol. 27, pp. 4–8.

Appendix

The temperature profile in the Newtonian fluid layer is given by

$$\Theta_N = \Theta_{HB}(0) - C_1 y + Pe_N^T \left[V_{HB}(0) \frac{y^2}{2} + \frac{Ma_N}{\mu} \frac{y^3}{6} + \frac{\delta}{12\mu} \left(\frac{y^5}{10} - \frac{y^4}{2} + y^3 \right) \right], \quad y \in [0, d],$$

where $C_1 = q_T - Pe_N^T \left(V_{HB}(0)\, d + \frac{Ma_N}{\mu} \frac{d^2}{2} + \frac{\delta}{2\mu} \left(\frac{d^4}{12} - \frac{d^3}{3} + \frac{d^2}{2} \right) \right)$.

The velocity and the temperature profiles in Herschel-Bulkley fluid are given by (31) and (34) respectively. For the case of Bingham fluid, n = 1, these integral presentations can be simplified. The results are given below for various flow regimes, which are numbered according to section 3 (see Fig. 2)

1. Entirely yielded, 1a.

$$V_{HB} = \frac{y^3+1}{6} - B\frac{y^2-1}{2} + M(y+1), \quad y \in [-1,0]$$

$$\Theta_{HB} = Pe_{HB}^T \left[\frac{1}{6} \left(\frac{y^5}{20} + \frac{y^2}{2} - \frac{9}{20} \right) - \frac{B}{2} \left(\frac{y^4}{12} - \frac{y^2}{2} + \frac{5}{12} \right) + M \left(\frac{y^3}{6} + \frac{y^2}{2} - \frac{1}{3} \right) \right] - \kappa C_1 (y+1),$$

2. Entirely unyielded, 1b.

$$V_{HB} = 0, \quad \Theta_{HB} = -\kappa C_1 (y+1), \quad y \in [-1,0]$$

Herschel-Bulkley flows if $|\tau_{HB}| > Bn$. The pass from yielded to unyielded regime can occur at $y = a, b, c$ or h, where $a = B + \sqrt{B^2 - 2(M - Bn)}$, $b = B + \sqrt{B^2 - 2(M + Bn)}$, $c = B - \sqrt{B^2 - 2(M + Bn)}$ and $h = B - \sqrt{B^2 - 2(M - Bn)}$.

3. Two layers, lower one is yielded, 2a

We define the depth of unyielded region by d_1, $-1 < d_1$ (a or c) < 0.

$$V_{HB} = \begin{cases} \frac{y^3+1}{6} - B\frac{y^2-1}{2} + M(y+1), & y \in [-1, d_1] \\ \frac{d_1^3+1}{6} - B\frac{d_1^2-1}{2} + M(d_1+1) = V_1, & y \in [d_1, 0] \end{cases}$$

$$\Theta_{HB}(y) = \begin{cases} \Theta_{HB,1}(y), & y \in [-1, d_1] \\ \Theta_{HB,2}(y), & y \in [d_1, 0] \end{cases}$$

$$\Theta_{HB,1} = Pe_{HB}^T \left[\frac{1}{6} \left(\frac{y^5}{20} + \frac{y^2}{2} - \frac{9}{20} \right) - \frac{B}{2} \left(\frac{y^4}{12} - \frac{y^2}{2} + \frac{5}{12} \right) + M \left(\frac{y^3}{6} + \frac{y^2}{2} - \frac{1}{3} \right) \right] + C_2(y+1), \quad y \in [-1, d_1]$$

$$C_2 = -\kappa C_1 + V_1 Pe_{HB}^T d_1 - Pe_{HB}^T \left[\frac{1}{6} \left(\frac{d_1^4}{4} + d_1 \right) - \frac{B}{2} \left(\frac{d_1^3}{3} - d_1 \right) + M \left(\frac{d_1^2}{2} + d_1 \right) \right]$$

$$\Theta_{HB,2} = V_1 Pe_{HB}^T \frac{(y^2 - d_1^2)}{2} - \kappa C_1 (y - d_1) + \Theta_{HB,1}(d_1), \quad y \in [d_1, 0]$$

3. Two layers, lower one is unyielded, 2b

Let d_1 be the depth of yielded region, -1 < d_1 (b or h) < 0, then

$$V_{HB} = \begin{cases} 0 & y \in [-1, d_1] \\ \frac{y^3 - d_1^3}{6} - B\frac{y^2 - d_1^2}{2} + M(y - d_1), & y \in [d_1, 0] \end{cases}$$

$$\Theta_{HB}(y) = \begin{cases} \Theta_{HB,1}(y) = C_3(y+1), & y \in [-1, d_1] \\ \Theta_{HB,2}(y), & y \in [d_1, 0] \end{cases},$$

$$C_3 = Pe_{HB}^T \left[\frac{1}{8} d_1^4 - \frac{\mathrm{B}}{3} d_1^3 + \frac{\mathrm{M}}{2} d_1^2 \right] - \kappa C_1,$$

$$\begin{cases} \Theta_{HB,2} = Pe_{HB}^T \left[\frac{1}{6} \left(\frac{y^5}{20} - d_1^3 \frac{y^2}{2} \right) - \frac{B}{2} \left(\frac{y^4}{12} - d_1^2 \frac{y^2}{2} \right) + M \left(\frac{y^3}{6} - d_1 \frac{y^2}{2} \right) \right] - \kappa C_1 y + C_4, \\ C_4 = C_3 (d_1 + 1) - Pe_{HB}^T \left[-\frac{3}{40} d_1^5 + \frac{5B}{24} d_1^4 - \frac{M}{3} d_1^3 \right] - \kappa C_1 d_1 \end{cases}$$

3. Three layers, lower one is yielded, 3a

Let the unyielded region lay between d_1 and d_2, –1 < d_1< d_2< 0. In this case d_1 and d_2 can be a and b or c and d.

$$V_{HB} = \begin{cases} \mathrm{sign}(\tau_1) \left[\frac{y^3 + 1}{6} - B\frac{y^2 - 1}{2} + M(y+1) \right], & y \in [-1, d_1] \\ \mathrm{sign}(\tau_1) \left[\frac{d_1^3 + 1}{6} - \mathrm{B}\frac{d_1^2 - 1}{2} + \mathrm{M}(d_1 + 1) \right] = V_1, & y \in [d_1, d_2] \\ \mathrm{sign}(\tau_3) \left[\frac{y^3 - d_2^3}{6} - \mathrm{B}\frac{y^2 - d_2^2}{2} + \mathrm{M}(y - d_2) \right] + V_1, & y \in [d_2, 0] \end{cases}$$

Here and further denotes the sign of shear stress function at the yielded (unyielded) region i.

$$\Theta_{HB} = \begin{cases} \Theta_{HB,1}(y), & y \in [-1, d_1] \\ \Theta_{HB,2}(y), & y \in [d_1, d_2] \\ \Theta_{HB,3}(y), & y \in [d_2, 0] \end{cases}$$

$$\begin{aligned} \Theta_{HB,1} =& Pe_{HB}^T \mathrm{sign}(\tau_1) \left[\frac{1}{6} \left(\frac{y^5}{20} + \frac{y^2}{2} - \frac{9}{20} \right) - \frac{B}{2} \left(\frac{y^4}{12} - \frac{y^2}{2} + \frac{5}{12} \right) + M \left(\frac{y^3}{6} + \frac{y^2}{2} - \frac{1}{3} \right) \right] \\ &+ C_5 (y+1), \\ C_5 =& - Pe_{HB}^T \mathrm{sign}(\tau_1) \left[-\frac{1}{8} d_1^4 + \frac{B}{3} d_1^3 - \frac{M}{2} d_1^2 \right] \\ &- Pe_{HB}^T \mathrm{sign}(\tau_3) \left[-\frac{1}{8} d_2^4 + \frac{\mathrm{B}}{3} d_2^3 - \frac{\mathrm{M}}{2} d_2^2 \right] - \kappa C_1 + V_1 Pe_{HB}^T (d_1 - d_2) \end{aligned}$$

$$\Theta_{HB,2} = V_1 Pe_{HB}^T \frac{y^2}{2} + C_6 y + C_7,$$

$$C_6 = -Pe_{HB}^T \text{sign}(\tau_3) \left[-\frac{1}{8} d_2^4 + \frac{B}{3} d_2^3 - \frac{M}{2} d_2^2 \right] - Pe_{HB}^T V_1 d_2 - \kappa C_1,$$

$$C_7 = \Theta_{HB,1}(d_1) - C_6 d_1 - V_1 Pe_{HB}^T d_1^2/2$$

$$\Theta_{HB,3} = Pe_{HB}^T \text{sign}(\tau_3) \left[\frac{1}{6} \left(\frac{y^5}{20} - d_2^3 \frac{y^2}{2} \right) - \frac{B}{2} \left(\frac{y^4}{12} - d_2^2 \frac{y^2}{2} \right) + M \left(\frac{y^3}{6} - d_2 \frac{y^2}{2} \right) \right] + Pe_{HB}^T V_1 \frac{y^2}{2} - \kappa C_1 y + C_8,$$

$$C_8 = \text{sign}(\tau_3) \left[-\frac{3}{40} d_2^5 + \frac{5B}{24} d_2^4 - \frac{M}{3} d_2^3 \right] - Pe_{HB}^T V_1 \frac{d_2^2}{2} + \Theta_{HB,2}(d_2) + \kappa C_1 d_2$$

3. Three layers, lower one is unyielded, 3b

Yielded region is between $d_1 = b$ and $d_2 = c$. $-1 < d_1 < d_2 < 0$.

$$V_{HB} = \begin{cases} 0, & y \in [-1, d_1] \\ \text{sign}(\tau_2) \left[\frac{y^3 - d_1^3}{6} - B \frac{y^2 - d_1^2}{2} + M(y - d_1) \right], & y \in [d_1, d_2] \\ \text{sign}(\tau_2) \left[\frac{d_2^3 - d_1^3}{6} - B \frac{d_2^2 - d_1^2}{2} + M(d_2 - d_1) \right] = V_1, & y \in [d_2, 0] \end{cases}$$

$$\Theta_{HB}(y) = \begin{cases} \Theta_{HB,1}(y) = C_9(y+1), & y \in [-1, d_1] \\ \Theta_{HB,2}(y), & y \in [d_1, d_2] \\ \Theta_{HB,3}(y), & y \in [d_2, 0] \end{cases}$$

$$C_9 = -Pe_{HB}^T \text{sign}(\tau_2) \left[\frac{1}{6} \left(\frac{d_2^4}{4} + d_1^3 d_2 \right) - \frac{B}{2} \left(\frac{d_2^3}{3} - d_1^2 d_2 \right) + M \left(\frac{d_2^2}{2} - d_1 d_2 \right) \right] + Pe_{HB}^T \text{sign}(\tau_2) \left[-\frac{1}{8} d_1^4 + \frac{B}{3} d_1^3 - \frac{M}{2} d_1^2 \right] + V_1 Pe_{HB}^T d_2 + \kappa C_1$$

$$\Theta_{HB,2} = Pe_{HB}^T \text{sign}(\tau_2) \left[\frac{1}{6} \left(\frac{y^5}{20} - d_1^3 \frac{y^2}{2} \right) - \frac{B}{2} \left(\frac{y^4}{12} - d_1^2 \frac{y^2}{2} \right) + M \left(\frac{y^3}{6} - d_1 \frac{y^2}{2} \right) \right] + C_{10} y + C_{11},$$

$$C_{10} = -Pe_{HB}^T \text{sign}(\tau_2) \left[\frac{1}{6} \left(\frac{d_2^4}{4} + d_1^3 d_2 \right) - \frac{B}{2} \left(\frac{d_2^3}{3} - d_1^2 d_2 \right) + M \left(\frac{d_2^2}{2} - d_1 d_2 \right) \right] + V_1 Pe_{HB}^T d_2 - \kappa C_1,$$

$$C_{11} = -Pe_{HB}^T \text{sign}(\tau_2) \left[-\frac{3}{40} d_1^5 + \frac{5B}{24} d_1^4 - \frac{M}{3} d_1^3 \right] + \Theta_{HB,1}(d_1) - C_{10} d_1$$

$$\Theta_{HB,3} = V_1 Pe_{HB}^T \frac{y^2}{2} - \kappa C_1 y + C_{12}, \quad C_{12} = \Theta_{HB,1}(d_2) - V_1 Pe_{HB}^T \frac{d_2^2}{2} + \kappa C_1 d_2$$

3. Four layers, lower one is yielded, 4a

$-1 < d_1 = a < d_2 = b < d_3 = c < 0$. Yielded regions are between -1 and d_1 and between d_2 and d_3,

$$V_{HB} = \begin{cases} \operatorname{sign}(\tau_1)\left[\frac{y^3+1}{6} - B\frac{y^2-1}{2} + M(y+1)\right], & y \in [-1, d_1] \\ \operatorname{sign}(\tau_1)\left[\frac{d_1^3+1}{6} - B\frac{d_1^2-1}{2} + M(d_1+1)\right] = V_1, & y \in [d_1, d_2] \\ \operatorname{sign}(\tau_3)\left[\frac{y^3-d_2^3}{6} - B\frac{y^2-d_2^2}{2} + M(y-d_2)\right] + V_1, & y \in [d_2, d_3] \\ \operatorname{sign}(\tau_3)\left[\frac{d_3^3-d_2^3}{6} - B\frac{d_3^2-d_2^2}{2} + M(d_3-d_2)\right] + V_1 = V_2, & y \in [d_3, 0] \end{cases}$$

$$\Theta_{HB}(y) = \begin{cases} \Theta_{HB,1}(y), & y \in [-1, d_1] \\ \Theta_{HB,2}(y), & y \in [d_1, d_2] \\ \Theta_{HB,3}(y), & y \in [d_2, d_3] \\ \Theta_{HB,4}(y), & y \in [d_3, 0] \end{cases}$$

$$\begin{aligned} \Theta_{HB,1} =& Pe_{HB}^T \operatorname{sign}(\tau_1)\left[\frac{1}{6}\left(\frac{y^5}{20} + \frac{y^2}{2} - \frac{9}{20}\right) - \frac{B}{2}\left(\frac{y^4}{12} - \frac{y^2}{2} + \frac{5}{12}\right) + M\left(\frac{y^3}{6} + \frac{y^2}{2} - \frac{1}{3}\right)\right] \\ &+ Pe_{HB}^T C_{13}(y+1), \\ \Theta_{HB,2} =& V_1 Pe_{HB}^T \operatorname{sign}(\tau_1)\frac{y^2}{2} + C_{14}y + C_{15}, \\ \Theta_{HB,3} =& Pe_{HB}^T V_1 \frac{y^2}{2} \\ &+ Pe_{HB}^T \operatorname{sign}(\tau_3)\left[\frac{1}{6}\left(\frac{y^5}{20} - d_2^3\frac{y^2}{2}\right) - \frac{B}{2}\left(\frac{y^4}{12} - d_2^2\frac{y^2}{2}\right) + M\left(\frac{y^3}{6} - d_2\frac{y^2}{2}\right)\right] \\ &+ C_{16}y + C_{17}, \\ C_{13} =& -\operatorname{sign}(\tau_1)\left[\frac{1}{6}\left(\frac{d_1^4}{4} + d_1\right) - \frac{B}{2}\left(\frac{d_1^3}{3} - d_1\right) + M\left(\frac{d_1^2}{2} - d_1\right)\right] - \\ &- \operatorname{sign}(\tau_3)\left[-\frac{1}{8}d_2^4 + \frac{B}{3}d_2^3 - \frac{M}{2}d_2^2 + \frac{1}{6}\left(\frac{d_3^4}{4} + d_2^3 d_3\right) - \frac{B}{2}\left(\frac{d_3^3}{3} - d_2^2 d_3\right) + M\left(\frac{d_3^2}{2} - d_2 d_3\right)\right] \\ &- V_1 d_2 - V_1 d_3 + V_2 d_3 - \kappa C_1 / Pe_{HB}^T + V_1(d_1 - d_2) \\ C_{14} =& -Pe_{HB}^T \operatorname{sign}(\tau_3)\left[-\frac{1}{8}d_2^4 + \frac{B}{3}d_2^3 - \frac{M}{2}d_2^2\right] - Pe_{HB}^T V_1 d_2 - \\ &- Pe_{HB}^T \operatorname{sign}(\tau_3)\left[\frac{1}{6}\left(\frac{d_3^4}{4} + d_2^3 d_3\right) - \frac{B}{2}\left(\frac{d_3^3}{3} - d_2^2 d_3\right) + M\left(\frac{d_3^2}{2} - d_2 d_3\right)\right] - \\ &- Pe_{HB}^T V_1 d_3 + V_2 Pe_{HB}^T d_3 - \kappa C_1 - V_1 Pe_{HB}^T d_2, \\ C_{15} =& \Theta_{HB,1}(d_1) - V_1 Pe_{HB}^T \frac{d_1^2}{2} - C_{14} d_1, \end{aligned}$$

$$C_{16} = -Pe_{HB}^{T}\operatorname{sign}(\tau_3)\left[\frac{1}{6}\left(\frac{d_3^4}{4}+d_2^3 d_3\right)-\frac{B}{2}\left(\frac{d_3^3}{3}-d_2^2 d_3\right)+M\left(\frac{d_3^2}{2}-d_2 d_3\right)\right]- \\ -Pe_{HB}^{T}V_1 d_3 + V_2 Pe_{HB}^{T} d_3 - \kappa C_1$$

$$C_{17} = -Pe_{HB}^{T}\operatorname{sign}(\tau_3)\left[-\frac{3}{40}d_2^5+\frac{5B}{24}d_2^4-\frac{M}{3}d_2^3\right]-Pe_{HB}^{T}V_1\frac{d_2^2}{2}-C_{16}d_2+\Theta_{HB,2}(d_2)$$

$$\Theta_{HB,4} = V_2 Pe_{HB}^{T}\frac{y^2}{2}-\kappa C_1 y + C_{18}, \quad C_{18} = \Theta_{HB,3}(d_3) - V_2 Pe_{HB}^{T}\frac{d_3^2}{2}+\kappa C_1 d_3$$

3. Four layers, lower one is unyielded, 4b

$-1 < d_1 = b < d_2 = c < d_3 = d < 0$. Yielded regions are between d_1 and d_2 and between d_3 and 0.

$$V_{HB} = \begin{cases} 0, & y\in[-1,d_1] \\ \operatorname{sign}(\tau_2)\left[\frac{y^3-d_1^3}{6}-B\frac{y^2-d_1^2}{2}+M(y-d_1)\right], & y\in[d_1,d_2] \\ \operatorname{sign}(\tau_2)\left[\frac{d_2^3-d_1^3}{6}-B\frac{d_2^2-d_1^2}{2}+M(d_2-d_1)\right]=V_1, & y\in[d_2,d_3] \\ \operatorname{sign}(\tau_4)\left[\frac{y^3-d_3^3}{6}-B\frac{y^2-d_3^2}{2}+M(y-d_3)\right]+V_1, & y\in[d_3,0] \end{cases}$$

$$\Theta_{HB}(y) = \begin{cases} \Theta_{HB,1}(y) = C_{19}(y+1), & y\in[-1,d_1] \\ \Theta_{HB,2}(y), & y\in[d_1,d_2] \\ \Theta_{HB,3}(y), & y\in[d_2,d_3] \\ \Theta_{HB,4}(y), & y\in[d_3,0] \end{cases}$$

$$C_{19} = Pe_{HB}^{T}\left\{\operatorname{sign}(\tau_2)\left[-\frac{3}{40}d_1^5+\frac{5B}{12}d_1^4-\frac{M}{3}d_1^3\right]+\operatorname{sign}(\tau_4)\left[-\frac{1}{8}d_3^4+\frac{B}{3}d_3^3-\frac{M}{2}d_3^2\right]\right\} \\ -\left[\frac{1}{6}\left(\frac{d_2^4}{4}+d_1^3 d_2\right)-\frac{B}{2}\left(\frac{d_2^3}{3}-d_1^2 d_2\right)+M\left(\frac{d_2^2}{2}-d_1 d_2\right)\right] \\ +Pe_{HB}^{T}-\kappa C_1 + V_1 Pe_{HB}^{T}(d_2-d_3),$$

$$\Theta_{HB,2} = Pe^T_{HB}\text{sign}(\tau_2)\left[\frac{1}{6}\left(\frac{y^5}{20}-d_1^3\frac{y^2}{2}\right)-\frac{B}{2}\left(\frac{y^4}{12}-d_1^2\frac{y^2}{2}\right)+M\left(\frac{y^3}{6}-d_1\frac{y^2}{2}\right)\right]$$
$$+C_{20}y+C_{21},$$
$$C_{20} = -\left[\frac{1}{6}\left(\frac{d_2^4}{4}+d_1^3d_2\right)-\frac{B}{2}\left(\frac{d_2^3}{3}-d_1^2d_2\right)+M\left(\frac{d_2^2}{2}-d_1d_2\right)\right]$$
$$+V_1Pe^T_{HB}(d_2-d_3)+Pe^T_{HB}\text{sign}(\tau_4)\left[-\frac{1}{8}d_3^4+\frac{B}{3}d_3^3-\frac{M}{2}d_3^2\right]-\kappa C_1,$$
$$C_{21} = \Theta_{HB,1}(d_1)-C_{20}d_1$$
$$-Pe^T_{HB}\text{sign}(\tau_2)\left[-\frac{3}{40}d_1^5+\frac{5B}{12}d_1^4-\frac{M}{3}d_1^3\right]$$
$$\Theta_{HB,3} = V_1Pe^T_{HB}\frac{y^2}{2}+C_{22}y+C_{23},\quad C_{22} = Pe^T_{HB}\text{sign}(\tau_4)\left[-\frac{1}{8}d_3^4+\frac{B}{3}d_3^3-\frac{M}{2}d_3^2\right]$$
$$-\kappa C_1-V_1Pe^T_{HB}d_3,\quad C_{23} = \Theta_{HB,2}(d_2)-V_1Pe^T_{HB}\frac{d_2^2}{2}-C_{22}d_2,$$
$$\Theta_{HB,4} = Pe^T_{HB}\text{sign}(\tau_4)\left[\frac{1}{6}\left(\frac{y^5}{20}-d_3^3\frac{y^2}{2}\right)-\frac{B}{2}\left(\frac{y^4}{12}-d_3^2\frac{y^2}{2}\right)+M\left(\frac{y^3}{6}-d_3\frac{y^2}{2}\right)\right]$$
$$+Pe^T_{HB}V_1\frac{y^2}{2}-\kappa C_1y+C_{24},$$
$$C_{24} = \Theta_{HB,3}(d_3)+\kappa C_1d_3-Pe^T_{HB}\left[\text{sign}(\tau_4)\left(-\frac{3}{40}d_3^5+\frac{5B}{12}d_3^4-\frac{M}{3}d_3^3\right)-V_1\frac{d_3^2}{2}\right]$$

3. Five layers, 5a

$-1 < d_1{=}a < d_2{=}b < d_3{=}c < d_4{=}h < 0$. Yielded regions are between -1 and d_1, d_2 and d_3, and between d_4 and 0.

$$V_{HB} = \begin{cases} \text{sign}(\tau_1)\left[\frac{y^3+1}{6}-B\frac{y^2-1}{2}+M(y+1)\right], & y\in[-1,d_1] \\ \text{sign}(\tau_1)\left[\frac{d_1^3+1}{6}-B\frac{d_1^2-1}{2}+M(d_1-1)\right]=V_1, & y\in[d_1,d_2] \\ \text{sign}(\tau_3)\left[\frac{y^3-d_2^3}{6}-B\frac{y^2-d_2^2}{2}+M(y-d_2)\right]+V_1, & y\in[d_2,d_3] \\ \text{sign}(\tau_3)\left[\frac{d_3^3-d_2^3}{6}-B\frac{d_3^2-d_2^2}{2}+M(d_3-d_2)\right]+V_1=V_2, & y\in[d_3,d_4] \\ \text{sign}(\tau_5)\left[\frac{y^3-d_4^3}{6}-B\frac{y^2-d_4^2}{2}+M(y-d_4)\right]+V_2, & y\in[d_4,0] \end{cases}$$

$$\Theta_{HB}(y) = \begin{cases} \Theta_{HB,1}(y), & y\in[-1,d_1] \\ \Theta_{HB,2}(y), & y\in[d_1,d_2] \\ \Theta_{HB,3}(y), & y\in[d_2,d_3] \\ \Theta_{HB,4}(y), & y\in[d_3,d_4] \\ \Theta_{HB,5}(y), & y\in[d_4,0] \end{cases}$$

$$\Theta_{HB,1} = Pe_{HB}^{T}\text{sign}(\tau_1)\left[\frac{1}{6}\left(\frac{y^5}{20}+\frac{y^2}{2}-\frac{9}{20}\right)-\frac{B}{2}\left(\frac{y^4}{12}-\frac{y^2}{2}+\frac{5}{12}\right)+M\left(\frac{y^3}{6}+\frac{y^2}{2}-\frac{1}{3}\right)\right]$$
$$+C_{25}(y+1),$$
$$C_{25} = -Pe_{HB}^{T}\text{sign}(\tau_1)\left[\frac{1}{6}\left(\frac{d_1^4}{4}+d_1\right)-\frac{B}{2}\left(\frac{d_1^3}{3}-d_1\right)+M\left(\frac{d_1^2}{2}-d_1\right)\right]-\kappa C_1$$
$$+Pe_{HB}^{T}\text{sign}(\tau_3)\left[-\frac{1}{8}\left(d_2^4-d_4^4\right)+\frac{B}{3}\left(d_2^3-d_4^3\right)-\frac{M}{2}\left(d_2^2-d_4^2\right)\right]+V_1 Pe_{HB}^{T}(d_1-d_2)$$
$$-Pe_{HB}^{T}\text{sign}(\tau_5)\left[-\frac{1}{8}d_4^4+\frac{B}{3}d_4^3-\frac{M}{2}d_4^2\right]+V_2\left[d_4\left(1-Pe_{HB}^{T}\right)-d_3 Pe_{HB}^{T}\right]?$$
$$\Theta_{HB,2} = V_1 Pe_{HB}^{T}\frac{y^2}{2}+C_{26}y+C_{27},\quad C_{26} = V_2\left[d_4\left(1-Pe_{HB}^{T}\right)-d_3 Pe_{HB}^{T}\right]-\kappa C_1 - V_1 Pe_{HB}^{T} d_2$$
$$+Pe_{HB}^{T}\text{sign}(\tau_3)\left[-\frac{1}{8}\left(d_2^4-d_4^4\right)+\frac{B}{3}\left(d_2^3-d_4^3\right)-\frac{M}{2}\left(d_2^2-d_4^2\right)\right]$$
$$+Pe_{HB}^{T}\text{sign}(\tau_5)\left[-\frac{1}{8}d_4^4+\frac{B}{3}d_4^3-\frac{M}{2}d_4^2\right],\quad C_{27} = \Theta_{HB,1}(d_1)-V_1 Pe_{HB}^{T}\frac{d_1^2}{2}-C_{26}d_1,$$
$$\Theta_{HB,3} = Pe_{HB}^{T}\text{sign}(\tau_3)\left[\frac{1}{6}\left(\frac{y^5}{20}-d_2^3\frac{y^2}{2}\right)-\frac{B}{2}\left(\frac{y^4}{12}-d_2^2\frac{y^2}{2}\right)+M\left(\frac{y^3}{6}-d_2\frac{y^2}{2}\right)\right]$$
$$+Pe_{HB}^{T}V_1\frac{y^2}{2}+C_{28}y+C_{29},$$
$$C_{28} = Pe_{HB}^{T}\text{sign}(\tau_5)\left[-\frac{1}{8}d_4^4+\frac{B}{3}d_4^3-\frac{M}{2}d_4^2\right]$$
$$+V_2\left[d_4\left(1-Pe_{HB}^{T}\right)-d_3 Pe_{HB}^{T}\right]-\kappa C_1 - Pe_{HB}^{T}\text{sign}(\tau_3)\left[-\frac{1}{8}d_3^4+\frac{B}{3}d_3^3-\frac{M}{2}d_3^2\right],$$
$$C_{29} = \Theta_{HB,2}(d_2)-C_{28}d_2 - Pe_{HB}^{T}\text{sign}(\tau_3)\left[-\frac{3}{40}d_2^5+\frac{5B}{12}d_2^4-\frac{M}{3}d_2^3\right]-Pe_{HB}^{T}V_1\frac{d_2^2}{2}$$
$$\Theta_{HB,4} = V_2 Pe_{HB}^{T}\frac{y^2}{2}+C_{30}y+C_{31},\quad C_{30} = Pe_{HB}^{T}\text{sign}(\tau_5)\left[-\frac{1}{8}d_4^4+\frac{B}{3}d_4^3-\frac{M}{2}d_4^2\right]$$
$$+V_2 d_4(1-Pe_{HB}^{T})-\kappa C_1,\quad C_{31} = \Theta_{HB,3}(d_3)-V_2 Pe_{HB}^{T}\frac{d_3^2}{2}-C_{30}d_3,$$
$$\Theta_{HB,5} = Pe_{HB}^{T}\text{sign}(\tau_5)\left[\frac{1}{6}\left(\frac{y^5}{20}-d_4^3\frac{y^2}{2}\right)-\frac{B}{2}\left(\frac{y^4}{12}-d_4^2\frac{y^2}{2}\right)+M\left(\frac{y^3}{6}-d_4\frac{y^2}{2}\right)\right]$$
$$+Pe_{HB}^{T}V_2\frac{y^2}{2}-\kappa C_1 y+C_{32},\quad C_{32} = \Theta_{HB,4}(d_4)+\kappa C_1 d_3$$
$$-Pe_{HB}^{T}\left\{\text{sign}(\tau_5)\left[-\frac{3}{40}d_4^5+\frac{5B}{12}d_4^4-\frac{M}{3}d_4^3\right]-V_1\frac{d_4^2}{2}\right\}.$$